Final Report

NASA Ames Cooperative Agreement. NCC 2-357

Report for the period Oct 1985 to Sept 1989

by

Dr. Sreedhara V. Murthy

Flow Unsteadiness Effects on Boundary Layers

Principal Investigator: Dr. Sreedhara V. Murthy

Recipient Institution: University of the Pacific
(Dept of Mechanical Engineering)
3601, Pacific Ave, Stockton, CA 95211

Final Report

NASA Ames Co-op Agreement No. NCC 2–357

Report for the period October 1985 to September 1989
by
Dr. Sreedhara V. Murthy

Flow Unsteadiness Effects on Boundary Layers

Principal Investigator: V Sreedhara Murthy
Dr. Sreedhara V. Murthy

Recipient Institution: University of the Pacific
(Department of Mechanical Engineering)
3601, Pacific Avenue, Stockton, CA 95211

Submitted to: *Dr. Frank W. Steinle*
Chief, Aerodynamic Facilities Branch *Code RAF*
NASA Ames Research Center, Moffett Field, CA 94035

Copy to: NASA Scientific and Technical Information Facility
P.O. Box 8757
Baltimore/Washington International Airport, Maryland 21240

Overall Objectives

University and Ames personnel would collaborate on performance of research to develop qualitative and quantitative understanding of the development of boundary layers at high subsonic speeds in the presence of either mass flux fluctuations or acoustic disturbances or both.

Contents

1 Background

The research tasks identified in this Co-operative Agreement emerged from the need to generate new inputs to the design database of advanced technology concepts such as advanced aircraft wing shapes, special types of rotorcraft aerodynamic configurations, and Laminar Flow Control techniques. The inputs from the project were to be in the subject area of boundary layer transition and growth at high subsonic and transonic flow speeds, particularly relating to the effects of freestream mass flux fluctuations and acoustic disturbances *(the two most important parameters in the flow unsteadiness environment affecting the aerodynamics of a flight vehicle).* Existing knowledge in this area was rather limited in terms of both computational prediction techniques and wind tunnel data updating capabilities.
With regard to the computational techniques, the quantum advancement that has occurred during the recent years in computational concepts could not be fully exploited for providing the desired level of confidence in predicted aerodynamic data, primarily because of the absence of a sufficiently detailed database that could inspire proper modeling of the transitional and turbulent states of boundary layers. Also, there existed only very limited information on the effects of many types of flow disturbances such as those generated by propulsive units, air intakes, protrusions, etc on the boundary layer developing over wing surfaces.
In contrast to this status on computational techniques, the situation with respect to wind tunnel data application capabilities and correction methodologies was not very different. A moderate level of understanding had been achieved, notably on the effects of tunnel wall interference, model and support system blockage,etc, but very little was known about the individual effects of free-stream flow-unsteadiness components, namely acoustic noise and turbulence, in the measured aerodynamic data.

The limitations in prediction capabilities and wind tunnel data updating procedures had meant that the complement of flight testing in aerospace vehicle development programs would remain almost prohibitively large. A better, high quality research database was needed to serve as a basis for constructing and validating new improved computational techniques, and to evaluate or update wind tunnel data application methodologies.

It was recognized that the new high quality research database must fully reflect the many ways in which the wind tunnel flow environment differed from the flight environment. Basically the difference between the two environments may be characterized by three flow quality parameters: freestream turbulence, pressure fluctuations, and temperature spottiness. (*see Fig-1*). The levels and spectra of these parameters would be related to the flow disturbance sources, namely, *fan rotation, flow turning at bends, wall boundary layer, wall geometry, and model support* in the case of wind tunnels, and *gusty winds, temperature gradients, clear air turbulence, and influence from other parts of aircraft*, in the case of flight. Data from each wind tunnel corresponds to a given combination of these parameters, as those exist in that tunnel. In order to apply this data to a flight environment composed of a different combination of flow quality parameters or to compare it with data from another wind tunnel, the best procedure was to apply corrections, one step at time, to the data for the differences in each of the individual flow quality parameters. To do so, it was essential to start from a database that provided the individual influences of these parameters. Of primary interest was the database on boundary layer transition phenom-

ena. Typically, with properly applied corrections, the location of transition would be correctly predicted, and the rest of the flowfield on a wing profile would also be adequately mapped (*see Fig.2*). A good, high quality database was therfore the key to successful predictions. The present Co-operative Agreement research project was specially aimed at generating such a high quality database, say, for generating detailed information concerning free-stream flow unsteadiness effects on boundary layer growth and transition in high subsonic and transonic speed ranges.

In specific terms, the Co-operative Agreement was intended to generate the desired database with a two-pronged approach: *(i)* from a detailed review of existing literature on research and wind tunnel calibration database, and *(ii)* from detailed tests in a special apparatus, namely the *Boundary Layer Apparatus for Subsonic and Transonic flow Affected by Noise Environment, ('BLASTANE')*, available at the Aerodynamics Division of NASA Ames Research Center. For the tests in BLASTANE, special instrumentation, including hot wire anemometry, the buried wire gage technique, and laser velocimetry, were to be used to obtain skin friction and turbulent shear stress data all along the laminar, transitional and turbulent stages of boundary layer growth, for various free-stream noise levels, turbulence content, and pressure gradients. This data base would then be useful for improving the correction methodology of applying wind tunnel test data to flight predictions and further would be helpful in providing pointers for making improvements in turbulence modeling laws.

2 Review of Existing Literature

Research literature relating to the results of recent investigations was reviewed in order to obtain a better insight into the effects of different flow parameters on boundary layer transition phenomena at high subsonic and transonic speeds.

With respect to the existing database, it was noted that, a series of detailed tests on the standard '*Ten-Degree Cone*' in several major wind tunnels had provided many pointers to the effects of flow unsteadiness levels in wind tunnels. A detailed review co-authored by the principal investigator showed that the existing database on the ten–degree cone did not fully clarify some of the important questions pertaining to the effects of the different flow unsteadiness components on boundary layer growth and transition phenomenon (*see Publication Nos. 1 and 2*). The review pointed out that the data base presented only the combined effects of acoustic noise, its frequency content, free-stream turbulence and Mach number, as those existed in the different wind tunnels participating in the ten–degree cone database effort.

The review further revealed that scatter in the data did not permit firm conclusions about the individual effects of the different flow variables. However, it was possible to propose new correlations that could act as guidelines to further effort in this area.

The detailed review began with a look at the theoretical methods. Earlier researchers had determined that the relationship between the so-called critical Reynolds number from infinitesimal disturbance stability theory and the actual transition Reynolds number was weak quantitatively and only moderately strong qualitatively. From the present author's view-point, this was to

be expected because the stability theory can only give pointers to the prediction of point of instability, but cannot provide a reliable basis for predictions of conditions further downstream where the disturbances will have grown to levels that are typical to a turbulent state. It was concluded that the existing theoretical methods need to be be updated, perhaps by first constructing new stability and disturbance–growth criteria, then validating those criteria in the context of research data from experiments, and finally, incorporating such new criteria in the boundary layer growth calculations. This meant that a new high quality experimental research database, of the type contemplated in the present project, was a pre-requisite. In the meantime, the principal investigator therfore decided to attempt new empirical correlations.

The methods used by earlier researchers for arriving at their conclusions seemed to indicate that they had concentrated on correlations with pressure fluctuation level and unit Reynolds number. The principal investigator reviewed the existing literature with a wider interpretation, and was able to postulate some new thoughts with respect to the possibilities of other correlations; say, with respect to the effect of Mach number, and the role of vorticity as an independent parameter compared to acoustic disturbances. These thoughts were basically triggered by the database from flight tests of the so-called *standard AEDC Ten Degree Cone* which was also subject to a series of detailed tests in many large wind tunnels (*see Fig.3*). Additional support to these thoughts came by way of the data from some of the wind tunnels that had comparatively low flow unsteadiness levels.

In order to postulate new correlations, the principal investigator attempted first to establish an empirical correlation for the effects of Mach number alone, separate from other parameters (vorticity and acoustic fluctuations).
Clearly, the entire database could not be used for the reason that much of the database had significant influences of other flow parameters that affect the transition phenomena. Out of the data base, a part that corresponded to relatively low levels of disturbance was extracted and examined for Mach number correlation. Mach number of 0.8 was arbitrarily taken as the reference Mach number. With respect to transition Reynolds number, the average of measured transition Reynolds numbers at Mach 0.8 in a given facility was taken as the reference transition Reynolds number for the data from that facility. The data was presented in a special format as seen in the reproduced figure (*see Fig.4*) in this report. The format of the figure was chosen to provide a convenient display of the Mach number trend for transition Reynolds numbers. Flight data, as seen in the figure, was shown as an envelope (hatched area) because the number of measurements is too large to reproduce individually. All the data in figure corresponded to low levels of disturbance - low to the extent that the pressure fluctuation levels (ratio of root mean square value of pressure fluctuations to the flow dynamic pressure) are less than one percent. The choice of one percent, rather than a lower value was derived from the desire to have a reasonably large sample of data. It was clear from the figure that both the beginning-of and the end-of transition Reynolds numbers are affected by Mach number. Given the spread in the flight data and the scatter in the wind tunnel test data, it was considered best to conclude that the effect of Mach number on either the beginning-of or end-of transition Reynolds numbers could be considered linear, with a correlation slope of 3 million per unit increment of Mach number.

The following correlation between the beginning-of or end-of-transition Reynolds number, $Re_{t\ or\ T}$, and Mach number, M, was thus evolved from the figure:

$$\frac{\delta Re_{t\ or\ T}}{\delta M} = 3 \times 10^6$$

This correlation formed the basis for defining an **"Equivalent Transition Reynolds number"**, $Re_{(t\ or\ T),equiv}$ that related each data point at different Mach numbers to a reference Mach number of 0.8.

$$Re_{(t\ or\ T),equiv} = Re_{t\ or\ T,atM} - (M - 0.8) \times 3 \times 10^6$$

It was important to subtract the effect of Mach number in this manner before examining the effects of flow disturbances because, for any desired Mach number, the existing database did not provide a large enough sample to help evaluate the effects of flow disturbance levels. With this thinking, it was possible to find new correlations with respect to the effects of pressure fluctuations and freestream turbulence. It may be noted here that earlier researchers had attempted correlations and come to the conclusion that both the beginning- and end-of-transition Reynolds numbers were correlated with pressure fluctuation level. But, in the present review, it was found that such a correlation was not quite satisfactory (*see Fig.5*). Once the effects of compressibility were subtracted from the data through the definition of the Equivalent Transition Reynolds Number, there seems to be no correlation at all for low noise levels, and no reliable correlation for higher levels (*see Fig.6*).
Having thus established that there is no acceptable correlation for pressure fluctuations, the next step was to examine the possibility of correlations with freestream turbulence.

Evidence of strong influence of free stream turbulence on boundary layers had been overwhelming. It was well known through extensive testing that an increase in the level of freestream turbulence would cause an increase in the amplification rates of flow disturbances, thus hastening transition. Influence of freestream turbulence was known to be significant all through the different stages of boundary layer (*laminar, transitional, and turbulent*). It was established that, with higher freestream turbulence, stability of laminar boundary layer was substantially reduced, onset of turbulence fluctuations in transition region was hastened, and skin friction along with other properties of turbulent boundary layer were significantly altered. It was thus very likely that freestream turbulence level would correlate well for transition Reynolds number.

A correlation plot was prepared for transition data from the wind tunnels for which freestream turbulence data was available. It became readily clear that both the beginning- and end-of-transition Reynolds numbers decreased with increasing freestream turbulence levels. The correlation plot was constructed with Equivalent Transition Reynolds Numbers to properly isolate the effects of Mach number (*see Fig.7*). The correlation laws could be postulated as:

$$Re_{(t\ or\ T),equiv}\ \alpha\ (\rho u)^{-n}_{rms\%}$$

$$with\ \ n = \frac{1}{4}\ for\ beginning\ of\ transition,\ and\ \ n = \frac{1}{6}\ for\ end\ of\ transition$$

Another correlation could also be derived for the effects of freestream turbulence. The ratio of beginning-of-transition to end-of-transition Reynolds numbers was related to freestream turbulence, but only weakly (*see Fig.8*):

$$\frac{Re_{t,equiv}}{Re_{T,equiv}} \alpha (\rho u)_{rms\%}^{-\frac{1}{12}}$$

It was an important step in the Cooperative Agreement project, that the review of existing literature made it possible to postulate new correlations for the effects of flow quality parameters. To further proceed and establish these new correlations, it was essential to obtain a better high quality database so that the scatter in data would not be a subject of argument with regard to the new correlation laws. The experimental part of the Cooperative Agreement was organized to provide this high quality database.

One other aspect relating to the effect of flow unsteadiness became evident during a review of the most recent flow measurements made in the NASA Ames 12 FT PWT entry-flow conditioning chamber. It became known that the characteristics of flow quality in the wind tunnel test section are dependent on a variety of factors, namely, the geometry of the bends, the turning vanes, the Contraction ratio, and the specific type of flow conditioning elements installed in the entry flow circuit. The influence of these factors appeared to be so varied that an appreciation of the flowfield emerging from the each individual flow-conditioning-device would be desirable in order to properly compose the full range of flow unsteadiness conditions that must be covered in the proposed studies of boundary layer transition phenomena. In this context, it is important to note that the unsteadiness in the flowfield emerging from the screens and honeycombs could be accompanied by a variation in mean velocity, which could then break-up into a turbulence field of its own, resulting in higher turbulence downstream. This would mean that standard turbulence decay law cannot be applied to obtain turbulence level at different stations in a wind tunnel test section, and therefore the turbulence field, *in terms of intensity and isotropy*, will have to be documented through a series of special experiments for that type of situation. Finally, the turbulence field entering a contraction is modified at the exit from contraction, but the effects are not always monotonic with respect to the contraction ratio.

It was decided that some studies ought to be made with respect to the characteristics of turbulence and velocity fields emerging from the different flow-conditioning devices commonly used in wind tunnels. A similar database was also needed for the NASA-Ames 12 FT PWT Restoration Project, and it was possible to combine the test requirements of the present research program with the data-base requirements of the 12 FT PWT project in such a way as to perform a single combined test program on a series of flow-conditioning elements.

3 Apparatus for Experiments

The experimental part of the Cooperative Agreement was an important part of the overall goals, and was organized with great care to provide a high quality database for the effects of flow quality parameters on boundary layer transition phenomena. The idea was to further develop a special apparatus, called *Boundary Layer Apparatus for Subsonic and Transonic flows Affected by Noise Environment ("BLASTANE")*, to a stage where it could be used to generate a variable flow environment suited to detailed studies on the effects of all the different parameters that influence the transition phenomena. It was recognized that the the main purpose for developing the apparatus *(BLASTANE)* was to establish a high quality database that would provide the basis for constructing a new method of comparing and correlating data from different wind tunnels and flight tests. In this regard, a critical requirement was that the apparatus must be of the variable configuration type, and must, at one end of the operating envelope, provide a very low flow unsteadiness level for base–line data generation. The apparatus would then be configured to provide varying levels of the different flow quality variables namely, compressibility, free-stream turbulence, pressure fluctuations, their frequency content, temperature spottiness, and pressure gradient.
The development targets of the apparatus were identified as:

Apparatus Development Targets

- To obtain flow surface accuracy and surface finish typical to those of Wind Tunnel Models.
- To achieve Mach Number range of up to Mach–1, higher Mach nos. if possible.
- To generate Varying Flow Unsteadiness Levels:
  - Acoustic Noise Level from Very Low to 3% in RMS Pressure Coeff.
  - Frequency Content from 100 Hz to 2 KHz.
  - Turbulence from Very Low to 3% RMS Mass Flux Fluctuations.

A brief description of the fully developed apparatus is given below:
The apparatus is very similar to a wind tunnel except for the one critical feature that the Test Section wall surface itself is to serve as the flow surface of interest for boundary layer studies and therefore had to be dimensionally very accurate and very smooth, typical to high speed wind tunnel model surfaces (*see Figs. 9, 10, 11*). Flow is induced by a vacuum source connected via a Diffuser section to the exit end of Test Section. The Diffuser has a diverging taper and accommodates a smoothly contoured Flow Control Plug that can be traversed along the centerline of the Diffuser to obtain different flow Mach numbers in the Test Section. For any desired Mach number in the Test Section, the Plug setting in the diverging passage of the Diffuser is so chosen as to ensure sonic "choking" of flow at the maximum diameter station of the plug, thus preventing any downstream disturbances from reaching the Test Section flow. Quality of flow in the Test Section then depends entirely on the conditions upstream in the Contraction section and the Settling Chamber.

BLASTANE Apparatus - Brief Description

ITEM	*DESCRIPTION*
Overall Type	• vacuum driven wind tunnel, choked (sonic) exit flow from test section. • long test section, smooth walls (low wall-induced disturbances)
Flow Speeds	• Test Section Mach= up to 1.0, atmospheric stagnation.
Test Section	• 10 inch dia., 72 inch long, very smooth wall surface.
Contraction	• 9:1
Settling Chamber	• fitted with desired number of screens to obtain variable turbulence levels. • fitted with an entry flange that can accommodate an electrically excited speaker for producing variable pressure fluctuation levels.
Air Intake Chr.	• fitted with filters to remove any contamination in entry air flow.

While performing preliminary tests to bring the BLASTANE apparatus to a fully operational status, it had become clear that the acoustic noise level in the room was rather excessive, large enough to cause a high pressure fluctuation level, *in excess of 95 dBA*, in the entry flow of the apparatus. This would adversely affect the capability to generate a complete set of baseline data on boundary layer flow for very low noise levels— a limitation which could not be accepted. Steps were therefore taken to reduce the noise level. The pipes and the bellows in the BLASTANE piping were wrapped with noise suppression material, and the noise level at the entry end of the Air Intake Chamber was reduced to less-than 85 dBA.

4 Instrumentation– Buried Wire Gages

Instrumentation consisted of conventional types, such as wall static pressure taps with a scanning transducer system, hot wire probes operated from constant temperature anemometer systems, and flush–mounted high response dynamic pressure transducers (*see Fig.12*). In addition, because of the need to generate a high quality database in the apparatus, it was necessary to develop special types of flow instrumentation to non-intrusively measure wall flow properties, such as wall shear stress. One very promising technique was the "Buried Wire Gage" technique which relied on the heated element concept for providing a measure of wall shear stress. The development of this technique consisted of first making reliable gages, and then calibrating those in a reliable flowfield. This development was a first–of–the–kind effort, and is described in the following sections.

4.1 General Aspects of Buried Wire Gage Technique

Buried Wire Gage Technique is based on the heated element concept which was conceived several decades ago; but, application of that concept in practical flow situations remained a formidable problem for a long time because of the lack of a proper sensor that could provide an adequate level of sensitivity.

Typically, the heated element concept consists of a sensing element that is arranged flush to the wall surface in a flow (*see Fig.13*). The element is heated to an appropriate temperature so that the characteristics of heat transferred to the wall layer of flow may be measured. However,

the heat transferred to the wall–flow layer is only a part of the total heat transfer that can be measured, namely the heat transferred away from the sensing element. The other part of the measured heat transfer is what is lost by thermal conduction to the substrate material surrounding the heated element. The proportion of heat transferred to the substrate material could be rather large for most choices of conventional substrate materials such as pyrex, quartz, plexiglas, etc, which are popularly used for "hot film" gages. With large losses to substrate, the sensitivity of flow measurement will suffer. Therefore, it was considered important that a proper choice be made for the substrate material.

Another aspect of the heated element concept that relies heavily on the characteristics of the sensor is the streamwise extent of the sensing element in the flow. Part of the measured heat transfer to wall layer of flow consists of the effects of local pressure gradients in the flow. These effects must be properly accounted for before the component of measured heat transfer relating solely to the wall flow friction may be extracted and converted to wall shear-stress. The pressure gradient component was known to be proportional to the streamwise extent of the sensing element and therefore could be reduced by making the sensing element appreciably slender.

The Buried Wire Gage technique seemed to satisfy both primary requirements: adaptability to low conductivity substrate materials, and very small streamwise extent. The gage consists of a very slender wire (a few microns in diameter) which is spot welded at its ends to a pair of electrical leads that are flush-embedded on a low thermal conductivity substrate. The wire is firmly attached to the substrate surface by a bonding process.

It was noted that the Buried Wire Gages are non-intrusive and readily provide a measure of the wall flow skin friction. Also such gages were known to have calibrations that were independent of the state of the boundary layer - laminar, transitional or turbulent.

4.2 Fabrication of Buried Wire Gages

The gages were developed specially to suit the instrument plugs that matched the test section walls of BLASTANE (*see Fig.14, 15*). Each plug was to be equipped with 5 gages at $\frac{1}{4}$ inch spacing. Each gage had a substrate insert with a very small sensor, a hot wire element, attached to it at the flow surface. The sensor was welded to electrical leads embedded in the substrate insert. The span of the sensor element was selected to be about $\frac{1}{16}$ inch. A 3–element gage with three sensor elements placed at close streamwise locations was also developed. The final method of making robust, reliable gages was carefully developed after a few unsuccessful trials. Basically, a reliable gage meant that the sensing element would not break, and the bond between the sensing element and the substrate surface would not deteriorate.

The development of the fabrication process began with selection of proper sensor and substrate materials, and was followed by a series of trials to determine a good bonding process that would keep the sensor well attached to the substrate surface.

The sensor had to be obviously small in size, durable, and robust. The best choice appeared to be a hot wire—tungsten wire of 4μ dia—which was readily available.

The substrate had to be of very low thermal conductivity to provide higher sensitivity in skin friction measurement. Polystyrene was the choice for this. The polystyrene was also available in the crystal form which could be used for injection molding, and thus accommodate electrical leads rather conveniently.

Bonding of the sensor element to the substrate had to be firm and durable. This was readily possible with polystyrene, for which a volatile solvent was available. The solvent bonding process simply means that a the solvent is to be dropped on the sensor so that the substrate material around the sensor would be dissolved and brought on the top of the sensor. As the solvent evaporated, the sensor would get covered with a thin layer of the substrate material. So, the procedure consisted of first injection-molding the substrate insert with leads, making sure that the substrate is frequently annealed so as to relieve any residual stresses, then welding the sensor to electrical leads, and finally solvent-bonding the sensor.

The finished instrument plug had five gages each (*see Fig.15*). The plug face diameter was 1.5". In all, a total of about 120 gages were built.

4.3 Calibration Law for Buried Wire Gages

The calibration law for a gage operated in the constant temperature mode, is independent of the state of boundary layer, and can be described as:

Buried Wire Gage Calibration Law

Gage operated in the Constant Temperature mode
Calibration independent of the state of Boundary Layer

$$\tau_w = 1.9 \frac{\mu^2 Nu^3}{\rho Pr B^2 d^2} - 0.2778 \frac{B d}{Nu} \frac{dp}{dx}$$

$$where, \qquad Nu = \frac{h_t}{k b (T_s - T_r)} - A \frac{k_{sub}}{k}$$

$A = Conduction\ Loss\ Factor,\ a\ calibration\ constant$

$B = Equivalent\ Length\ Factor,\ second\ calibration\ constant$

b = span of the sensor (wire length)
d = streamwise length of sensor (wire dia)
h_t = total heat rate transferred from sensor
k = thermal conductivity of flow medium
k_{sub} = thermal conductivity of substrate matl.
Nu = Nusselt number
p = freestream pressure
Pr = Prandtl number
T_r = sensor un-heated('recovery') temp.
T_s = sensor operating temp. (absolute)
x = streamwise distance.
ρ = density
τ_w = wall-flow skin friction
μ = absolute viscosity

A and B are the calibration constants, to be determined from measurements in a known flow. It is to be noted here that the constant A can be determined from a measurement in the absence of any flow. The constant B must be determined from measurement in a flow for which the skin friction is otherwise known.
One more step in the calibration process is not readily obvious, but is needed. This has to do with the manner by which the sensor temperature, both the operating temperature T_s and the "non-operating" flow-recovery temperature T_r may be determined. With the constant temperature anemometer system, it is always possible to measure the resistance values very accurately,

and if the sensor resistance–temperature relationship is available, the measured resistance values can be used to obtain the corresponding temperature values accurately.

Some application aspects of the technique are obvious from the calibration law itself. First, it is important that, for good sensitivity in measurements, the contribution of conduction loss to the substrate, the term associated with A, should be kept small. This is best accomplished by selecting a substrate material of very low thermal conductivity. The second aspect is the influence of any local pressure gradients. For that contribution to be small, the sensor length d in the streamwise direction should be small.

The calibration of each of the 120 gages consisted of a 3–step procedure.
The **first step** was to determine the resistance—temperature law of the sensor. This was accomplished by keeping the gages in a temperature controlled chamber and measuring the resistance values for various temperature settings.
The **second step** was to determine the Conduction Loss Factor, A. This was accomplished by operating the sensor from the anemometer system while the sensor was in the temperature controlled chamber. Operation of the sensor was similar to the operation of any standard hot wire sensor. The factor was determined for different sensor operating temperatures and for different chamber temperatures so as to obtain an average value for the Conduction Loss Factor (*see Figs.16, 17*).
The **final step** in the calibration procedure was to determine the flow-related constant, namely the Equivalent Length Factor. For this purpose, a pipe-flow apparatus, which consisted of a 3" dia pipe, about 56 diameters long, was used (*see Fig.18*). The length/diameter ratio of the pipe was large enough to assure a fully developed pipe-flow. The flow entering the pipe passed through a honeycomb and several screens so that the pipe flow would not develop any swirl component. The instrument plugs with the buried wire gages were to be installed in the calibration section. The flow passed from the calibration section to an exit pipe which was more than 10 diameters long so that the pipe flow pattern in the calibration section would be undisturbed. Flow speeds in the pipe was varied by changing the orifice plates at the exit end of the exit pipe. Flow was induced from a vacuum supply. Static pressure taps in and near the calibration section were used for measuring the pressure drop along flow length. This pressure drop was then converted to skin friction values by using standard pipe-flow governing equations, according to a method specially developed in this project, described below:

4.4 Data Reduction Method for Pipe–flow–based Calibrations

The needs of the calibration data reduction effort led to a thorough review of existing literature on pipe-flow, primarily to find a proper method for obtaining wall-flow skin-friction values from measured static pressure distributions in the presence of significant compressibility effects. Proper methods were not available, and it was decided to evolve and establish a new method for properly reducing the data collected in the present calibration tests. This new method consisted of a series of steps to account for the effects of compressibility in the flowfield. Velocity and density variations across the flow cross section were approximated by profile shapes recommended for flow past flat plates. The wall of the pipe was assumed to have attained an adiabatic condition. An integral–principle was used to obtain solutions for the governing equa-

tions of flow. This new data reduction method was then used to analyze the detailed pressure measurements made in the long pipe-flow section of the Calibration Tube apparatus for all the flow settings used in the calibration of the buried wire gages. Flow friction values derived from this analysis were compared with the standard incompressible pipe-flow data available in literature. A brief description of this work relating to pipe-flow is given below: (*see Publication No.6*).

Background on Pipe–Flow:

The pipe flow can be described by "u_c" the centerline velocity, "M_c" the centerline Mach number, "T_c" the centerline temperature, and, "p_1" the wall static pressure at station-'1' (*see Fig.19*). All of these variables change as the flow passes to a downstream station. The flowfield is to be defined in terms of these changes, as a function of the pipe diameter "d", flow development length "x", and distance normal to the wall "y".

As noted earlier, a thorough review of the literature on pipe-flow revealed that there was a need to generate a more extensive database for the pipe-flow because of the need to establish a better understanding of high subsonic pipe-flows, *(i.e., properly account for compressibility effects)*, use such an understanding for calibration aspects, and finally develop an improved modeling of compressible boundary layer flows.

For the case of incompressible flow, the flowfield is usually described in terms of an invariant velocity profile along the length of the pipe. The profile shape would change with Reynolds number based on the pipe diameter. The velocity profile would be described as a power—law, $u/u_c = [y/(d/2)]^n$, with the exponent "n" being a function of Reynolds number. The flow friction then becomes a very simple function of the wall pressure gradient.

$$Velocity\ Profile \cdots \quad \frac{u}{u_c} = [\ \frac{y}{d/2}\ ]^n = \eta^n$$

$$Flow\ Friction \cdots \quad \tau_w = -\frac{d}{4}\frac{\partial p}{\partial x}$$

However, with respect to Compressible pipe—flow, the existing analysis in published literature used some simplifying assumptions. The effects of these assumptions on the calculated flow friction values to be used in the calibrations of the Buried Wire gages was a matter of concern in the present project. The existing analysis treated the flowfield in terms of an "averaged" velocity or Mach number which would vary along the length of the pipe, and an invariant profile shape. Flow friction was derived as a function of pressure gradient and the "averaged" Mach number, (M_{ca}).

$$Velocity\ Profile \cdots \quad "AVERAGED"$$

$$Flow\ Friction \cdots \quad \tau_w = -\frac{d}{4}\ \frac{(1 - M_{ca}^2)}{[1 + (\frac{\gamma-1}{2})M_{ca}^2]}\ \frac{\partial p}{\partial x}$$

In order to include the details of the velocity profile and the changes that occur with Reynolds number, and thus ensure that the flow friction values derived from gage-calibration test measurements for the present project would be sufficiently accurate, it was necessary to develop a new analysis of the pipe-flow. The density profile was derived from the velocity profile by using well established relationships between temperature and velocity profiles for boundary layer flowfields. The flowfield was described in terms of a centerline Mach number that varied along the length of the pipe.

4.4.1 Pipe-flow Profile Definitions

The development of the new analysis method started with definition of some profile properties. Velocity profile was defined in the same way as for incompressible flow— a power law profile, with the exponent "n" being a function of Reynolds number.

$$Velocity\ Profile: \quad \frac{u}{u_c} = \left(\frac{y}{d/2}\right)^n = \eta^n$$

The temperature profile was then defined in the same way as for compressible flow boundary layers with adiabatic wall conditions. "r" is the recovery factor that accounts for the effects of compressibility.

$$Temperature\ Profile: \quad \frac{T}{T_c} = 1 + r\frac{\gamma - 1}{2} M_c^2 \left[1 - \left(\frac{u}{u_c}\right)^2\right]$$

Next, a series of profile integrals were defined to simplify the structure of pipe-flow governing equations. These integrals simply described the integral properties of the velocity and the density profile shapes. Using these definitions, it was possible to write the governing equations in one-dimensional integral forms.

- **Profile Integarals:**

$$\sigma_1 = \int_{\eta=0}^{\eta=1} 2\frac{\rho u}{\rho_c u_c}(1-\eta)\partial\eta \qquad \sigma_2 = \int_{\eta=0}^{\eta=1} 2\frac{\rho u^2}{\rho_c u_c^2}(1-\eta)\partial\eta$$

$$\sigma_3 = \int_{\eta=0}^{\eta=1} 2\frac{u}{u_c}(1-\eta)\partial\eta \qquad \sigma_4 = \int_{\eta=0}^{\eta=1} 2\frac{\rho u^3}{\rho_c u_c^3}(1-\eta)\partial\eta$$

4.4.2 Pipe-flow Governing Equations

The pipe-flow governing equations then took the following form:

Pipe-Flow Governing Equations

$$Continuity \cdots \frac{\partial}{\partial x}\left[\frac{p M_c \sigma_1}{\sqrt{T_c}}\right] = 0$$

$$Momentum \cdots \frac{\partial}{\partial x}\left[p\left(1 + \gamma\sigma_2 M_c^2\right)\right] + \frac{4}{d}\tau_w = 0$$

$$Energy \cdots \frac{\partial}{\partial x}\left[T_c\left(1 + \frac{\sigma_4}{\sigma_3}\frac{(\gamma-1)}{2} M_c^2\right)\right] = 0$$

These were fairly familiar forms of the Continuity, Momentum and Energy equations. The Continuity and the Energy equation were then combined to produce one combined equation, in the process defining a "Continuity Function, F" for convenience.

- **Combined Continuity and Energy**("Continuity Function")

$$\frac{\partial}{\partial x}\Big[\ pM_c\sigma_1\sqrt{1+\frac{\sigma_4}{\sigma_3}\frac{\gamma-1}{2}M_c^2}\ \Big] = \frac{\partial}{\partial x}[\ F\ ] = 0$$

This combined equation and the momentum equation were to be solved for obtaining the flow friction τ_w as a function of measured pressure distribution p.

4.4.3 Pipe-flow Profile Properties

In order to find solutions, it was necessary to provide a closure for the governing equations by evolving a procedure to complete the definitions of the profile integrals, $\sigma's$, in terms of the profile exponent. Incompressible pipe-flow database was used as the basis for prescribing the velocity profile.

Incompressible Turbulent Pipe-flow

$$VelocityProfile\cdots \quad \frac{u}{u_c} = [\ \frac{y}{d/2}\ ]^n$$

For incompressible pipe–flow, existing database had shown that the profile exponent "n" is a function of Reynolds number as shown in the tabulation below:

Reynolds No. (based on dia.)	Profile Exponent "n"
4.0×10^3	1/6
2.3×10^4	1/6.6
1.1×10^5	1/7
1.1×10^6	1/8.8
2.0×10^6	1/10
3.2×10^6	1/10

This relationship, for convenience, could be approximated as a continuous function of Reynolds number, as shown below:

$$Approximation\cdots \quad n = \frac{1}{7}\ [\ 1 - 0.19\ log(\frac{Re}{0.75\times 10^5})\ ]$$

This relationship was used for compressible flow also. The density profile could then be expressed as a function of the velocity profile exponent and Mach number, using standard compressible boundary layer relationships. Thus:

Compressible Turbulent Pipe-flow

Velocity Profile as in the case of incompressible flow.

$$Density\ Profile \cdots \quad \frac{\rho}{\rho_c} = 1 - 0.88\,\frac{\gamma-1}{2}\,M_c^2\,(1-\eta^{2n})$$

With these inputs, the governing equations described earlier, namely the combined Continuity/Energy Equation and the Momentum Equation, became closed and allowed a thorough analysis of the measurements in a pipe–flow to determine the flow friction values.

4.4.4 Pipe-flow Experiments and Validation of Data Reduction Method

It may be noted here for quick reference that the apparatus consisted of a 3-inch bore long tube, long enough to produce fully developed pipe–flow. Flow entry was made smooth with a bell–mouth contour, a honeycomb and several screens (*see Figs.18, 19*). An orifice plate device at the exit was used to accommodate different orifice plates for changing the flow speeds. The flow was always choked at the orifice plate. The apparatus had a separate segment as test region, and the match between these sections was better than 0.001-inch.
The experiments were always run with a high vacuum, to ensure that the flow was choked at the orifice plate, thus entirely eliminating the propagation of downstream disturbances to the test region.
Instrumentation consisted of wall pressure taps read on scani–valves. Some of the taps were also read from specially calibrated, more sensitive "PARO" transducers. A miniature total-head Pitot tube was used for measuring centerline total pressure and to thus obtain a calibration of the different Orifice plates in terms of Mach number in the test region.

Experiments and Data Analysis

The various steps used for analyzing the data is listed below:

1. Pressure data was smoothed using localized curve-fitting technique. *so that the scatter in measurements at adjacent locations do not cause large changes in pressure gradient values.*
2. Mach No. *vs.* Orifice dia were derived from Total and Static pressure values.
3. Velocity Profile Exponent values were derived thru interpolations described below:
   - A guessed value of "n" was inserted in the Energy Equation to obtain Center-line Temperature.
   - Center-line density was derived from perfect gas law.
   - Average Velocity (U_{mean}) values were obtained from the Center-line Mach, Temperature, and "n".
   - Reynolds number was then calculated from standard definitions:

$$Reynolds\ No. = \rho_c\, U_{mean}\, d/\mu_c$$

   - "n" was updated using the above Reynolds Number.

$$n = \frac{1}{7}\,[\,1 - 0.19\ log(\frac{Re}{0.75\times 10^5})\,]$$

4. "n" was assumed to be invariant over selected flow-length.

5. Combined Continuity/Energy Equation was used to obtain Mach No. distribution from pressure distribution.

6. Flow Friction values were then derived from Momentum Equation.

$$Flow\ Friction\ Coeff\ =\ C_f\ =\ \frac{\tau_w}{(1/2)\rho_c\ U_m^2}$$

7. The friction values were then compared with established Incompressible-flow (C_{fsi}) Law:

$$\frac{1}{\sqrt{4\ C_{fsi}}}\ =\ 2.0\ log(Re\ \sqrt{4\ C_{fsi}}\ )\ -\ 0.8$$

The final step 7 was simply an effort to validate the new data reduction method by comparing the data with the established flow friction law for incompressible flow in a smooth pipe. This step also provided an opportunity to derive the effects of compressibility in pipe-flow.
The measured pressure distributions were used for calculating the variation in Mach number along the length of the pipe. The pressure distribution and the Mach number distribution were displayed in the form of ratios with respect to the values at a chosen "reference" station. "x"-axis is the length along the pipe expressed in terms of pipe diameter. The pressure data was fitted with a second degree curve-fit for data smoothing as shown (*see Fig.20*). It was evident from the measured pressure values, which were actually a collection of data accumulated from different days and many tests, that the pressure data was well described by the curve-fit, with a fairly small scatter. It was decided that the curve-fit was a good method for smoothing the pressure data for obtaining flow friction values.

The flow friction coefficient values, derived by applying this new analysis method to the pressure data, was displayed as a function of the Reynolds number. The results were compared with the law established for incompressible flow in a smooth pipe. The difference between the least square error line fit for the present data and the incompressible pipe-flow law was identified as the effect of compressibility (*see Fig.21*). This difference was also presented in a different format by showing the flow fiction coefficient as a function of Mach number (*see Fig.22*). For obtaining clarity in the presentation of the Mach number effect, an additional step was adapted. The effect of Reynolds number was isolated from the present data by constructing the ratio of measured flow friction coefficient to the incompressible flow value for the same Reynolds number. Then a curve fit was used as an extrapolation method for obtaining the intercept of this ratio down to Mach—zero. This intercept was then used as the reference value for presenting the effect of Mach number. The "y"-axis in the Mach number correlation-figure was therefore a ratio of ratios (*see Fig.22*).
From this correlation figure, it was readily apparent that there was a significant effect of Mach number. The trend for Mach number was comparable to the observed trends for flat plate boundary layer flows, as seen from a least square fit to the present data and the flat plate data (*see Fig.22*). It was thus established that the influence of compressibility was the same for pipe-flow as for flat plate boundary layer flows.

Having thus established and validated a data reduction method for obtaining correct values of compressible pipe–flow skin friction, it was then possible to pursue the task of calibrating the buried wire gages for compressible flow speeds.

4.5 Apparatus for flow–Calibration of Buried Wire Gages

As mentioned earlier, the final step in the buried wire gage calibration procedure was to determine the flow-related constant, namely the Equivalent Length Factor. For this purpose, the pipe-flow apparatus *(a 3" dia pipe, about 56 diameters long)*, was used (*see Fig.18*). As mentioned earlier, the length/diameter ratio of the pipe was large enough to assure a fully developed pipe-flow. The flow entering the pipe was passed through a honeycomb and several screens so that the pipe flow would not develop any swirl component. The instrument plugs with the buried wire gages were installed in the calibration section. The plug mounting port was specially made to accommodate the 5 inch radius contoured surfaces of the instrument plug in such a way as to expose only the sensors to the pipe-flow flowline of 1.5" radius. The mounting had a slot with knife-edged sides and a properly contoured top face that would flush support the faces of the instrument plug. The sensor elements would then appear through the slot opening, to be flush to the wall flow in the calibration section *(see Fig.18)*.
The flow passed from the calibration section to an exit pipe which was more than 10 diameters long so that the pipe flow pattern in the calibration section would be undisturbed. Flow speeds in the pipe was varied from low subsonic to high subsonic speeds, by changing the orifice plates at the exit end of the exit pipe. Flow was induced from a vacuum supply. Static pressure taps in and near the calibration section were used for measuring the pressure drop along flow length. This pressure drop was then converted to skin friction values by using the pipe-flow data reduction method described in the earlier section of this report.

4.6 Flow Calibration of Buried Wire Gages

The gages were operated from an existing constant temperature anemometer system. This Anemometer system had a special operational feature called the *Overheat Reference Value (ORV) Function*, which provided an indication of the gage-sensor resistance in flow. This ORV capability could be used to a great advantage in the data acquisition process, — it could replace the need to undertake a time-consuming step of adjusting the control resistor of the system while determining the 'cold' resistance of the gage sensor. But, the suppliers of the anemometer system had not provided a calibration of this ORV feature. With a fully calibrated ORV feature, the anemometer could remain set on the operating resistance value while the ORV indicated by the 'NULL DISPLAY' function of the system could be noted for later use in deriving the 'cold' resistance value of the sensor. The 'cold' resistance value could then be used for obtaining the flow-related 'recovery' temperature, to be used in the calibration laws of the buried wire gage technique. As a part of the calibration experiments, all the sixteen channels of the anemometer system were calibrated for the ORV feature, and validated for measurement of the 'cold' resistance value. This new method of determining the 'cold' resistance was incorporated in the data reduction package, thus reducing the set-up time needed for taking a data point (*see Publication Nos. 4, 5*).

The total Nusselt number measured with the gages in these tests were plotted against the pipe–flow skin friction values derived from wall pressure measurements. The total Nusselt number represents the total heat rate delivered from the anemometer system to the sensor, and contains contribution from flow as well as conduction loss into substrate. The x-axis of this plot format was shifted for clarity (*see Figs.23*). The skin friction was shown in the form of a non-dimensional quantity based on the flow variables associated with it in the calibration law. The number includes the effects of local density. The results clearly validate the characteristics of the calibration law. The format of the figure also illustrates the effect of conduction loss on the sensitivity of measurements. The intercept at no-flow, *zero skin friction*, is relatively large even for the present choice of substrate (*see Figs.23*). It is therefore very important that the substrate be well chosen to keep the conduction loss to a minimum.

4.7 Buried Wire Gage Calibration Checks

Some of the gages were used for making extensive calibration checks, by operating those in the pipe-flow flowfield for a wide range of flow speeds. The calibration constants derived from earlier measurements in the pipe–flow were used for obtaining the flow–friction values. These measurements were compared with the actual flow–friction values determined form wall–pressure measurements. The comparison was very good, as could be seen from the tight cluster of data points on the line of perfect agreement (*see Figs.24*).

4.8 Calibration Constants of Typical Buried Wire Gages

Calibration constants, namely the Conduction Loss Factor A, and the Equivalent Length Factor B, of the entire 120 gages were reviewed in an effort to identify any opportunities for reductions in the calibration effort. The idea was to determine if, for gages which were identical in size, the calibration constants could be considered equal. As it happened, this was not the case. The differences in the calibration constant values were significant (*see Figs.25*).

In an attempt to further explore the opportunities for reductions in calibration effort, the gage calibration constants were placed on a cross–correlation plot (*see Figs.26*). The figure displayed the correlation plot for all the gages that were calibrated in the present effort. It was again clearly evident that the correlation was not tight enough to justify a carry-over procedure for calibration constants. The obvious conclusion was that each gage must be calibrated individually.

5 Instrumentation– Hot Wire Probes, Transducers, *etc.*

5.1 Hot Wire Probes

Hot wire probes were fabricated to allow measurements of freestream turbulence. Traversing screw-slides were mounted on a few Instrument Plugs so that a hot wire probe could be positioned at any desired distance from the wall layer of the flow.

5.2 Pressure Transducers

Pressure transducers were installed in a few of the Instrument Plugs to facilitate measurement of the fluctuating pressure level at the wall flow region (*see Figs.27*).

5.3 Data System

SWTS (Standard Wind Tunnel System), the data system of the NASA-Ames Unitary Wind Tunnel facilities, was the main source of acquiring and archiving the test data. A *PC-clone* was used for interfacing the anemometer system with the *SWTS* system.

Computer—controlled scanivalves were used in the initial series of preliminary tests to acquire wall static pressure distribution along the BLASTANE Test Section. After some attempts to overcome some of the operational and maintenance problems of the scani-valve system, it was decided to use an alternate pressure measurement system, namely the *'PSI' (Pressure Systems Inc.*©) electronically scanning pressure measurement system. Data from this system was also readily processed through the *SWTS* system.

6 Experiments

6.1 Preparation for Experiments

BLASTANE Apparatus

It may be noted for quick reference here that the BLASTANE (*Boundary Layer Apparatus for Subsonic and Transonic flow Affected by Noise Environment*) apparatus was made fully operational during the early stages of the term of the present Co-operative Agreement (*see Publication No. 3*). However, as mentioned earlier, it had become clear that the acoustic noise level in the room was rather excessive, large enough to cause a high pressure fluctuation level, *in excess of 95 dBA*, in the entry flow of the apparatus. It was known that this level of noise would adversely affect the capability to generate a complete set of baseline data on boundary layer flow for very low noise levels— a limitation which could not be accepted in the scope of the present Cooperative Agreement. Steps were therefore taken to reduce the noise level. The pipes and the bellows in the BLASTANE piping were wrapped with noise suppression material, and the noise level at the entry end of the Air Intake Chamber was reduced to less-than 85 dBA.

Buried Wire Gage Calibration Experiments

Activities relating to experiments included the setting up of the pipe–flow apparatus for a series of tests pertaining to calibration of the large number of buried wire gages. These tests have already been discussed in an earlier section of this report *(see section 4)*.

Flow Characterization Experiments

The next stage in the experimental program was to to extend the entry-flow length of the BLASTANE flow circuit (*see Publication No. 7*), so as to undertake tests relating to characterization of flow quality emerging from commonly used flow conditioning devices. Additional parts were designed for BLASTANE. These were to be capable of accommodating ring-inserts fitted with different samples of commonly used flow conditioning elements, such as screens of different mesh sizes and open-area ratios, honeycombs of different cell sizes, heat exchanger panels, etc. With these types of inserts, it was possible to introduce the different flow conditioning elements at any desired relative location in the BLASTANE flow circuit.

With respect to the **type of entry flow conditions** for which the flow conditioning elements must be tested, it was known that the overall flow pattern and the turbulence levels at entry to any typical turbulence reduction device in large wind tunnels would be highly non-uniform across the cross section. Based on data from many tunnels, in particular from the flow measurements in the NASA–Ames 12 FT PWT, it was expected that the flow velocity profile emerging from the wide angle diffuser, ahead of the turbulence reduction devices, would be typical to a separated-flow profile, with very low velocities near one wall and high velocities near the other wall *(see Fig.28)*. This flowfield would also exhibit large flow angles at entry to the Turbulence Reduction System *(TRS)* system. One other notable feature of such typical flowfield, as evidenced by the 12 FT PWT flow measurements, was that the turbulence levels and scale lengths

would be very large, obviously because those would have been inherited from the large dimensions of the flow passage, and the large size of turning vanes. It thus became clear that the entry flow conditions for the flow characterization tests should reflect large velocity gradients, high turbulence levels, and large length scales.

With respect to the different **flow conditioning element types** that need to be studied for the flow characterization tests, it was clear that screens and honeycombs must be included. The role of a heat exchanger was not clear. However, recent research had shown that typical heat exchangers could also be regarded as a part of the TRS. The present author reviewed existing literature on the flowfield emerging from a heat exchanger, and determined that the heat exchanger could be treated, and designed-in, as a part of the TRS. The author's review showed that the exit flow from a parallel plate type heat exchanger would be similar to the exit flow from a honeycomb, the characteristic length being the tube–spacing.

With the above reasoning, it was decided that the studies for characterization of the flowfield in large wind tunnels should include some studies of heat exchangers as a turbulence reduction element.

Prior to conducting tests on the flow characterization aspects, an attempt was made to examine the possibilities of computing the properties of the flowfield emerging from typical flow conditioning devices. However, given the complexity of a typical flowfield entering the TRS and the limitations of the existing literature *(and database)* on large–level flow variations, it was not possible to construct a reliable prediction method for calculating the properties of the flowfield at the exit from the TRS. More detailed data on TRS elements, with larger variations in entry flow properties, was needed in order to establish a reliable flowfield prediction method. It was therefore decided that the tests should be conducted rightaway.

The additional parts needed to extend the entry length of BLASTANE, and the ring inserts equipped with different types of flow conditioning elements were fabricated and assembled in the BLASTANE flow circuit. It is relevant to note here that the flow characterization tests were combined with another test program which was aimed at providing a database on turbulence reduction elements to be used in the NASA Ames 12 FT PWT restoration project. The additional parts brought the BLASTANE to the configuration described below:

Modified BLASTANE Apparatus - Brief Description (*see Fig.29*)

ITEM	*DESCRIPTION*
Overall Type	• vacuum driven wind tunnel, choked (sonic) exit flow from test section. • long test section, smooth walls (low wall-induced disturbances)
Flow Speeds	• Test Section Mach= 0.19 to 1.0, atmospheric stagnation.
Test Section	• 10 inch dia., 72 inch long, very smooth wall surface.
Contraction	• 20:1
Low-speed region	• long flow length with Flow Chambers, Probe Chambers.
Flow Chamber	• 6 chambers, 54 inch dia, 24 inch long, interchangeable location. • may be fitted with screen rings, honeycombs, frame-work, heat exchanger panels, wide angle diffuser models.
Probe Chamber	• 3 chambers, 45 inch dia, 24 inch long. • may be located between any two Flow Chambers. • has a traversing Probe-Strut with a Probe-head at the tip. • Pitot probes, 3-element and 1-element Hot Wire Probes, and other probes may be mounted in the Probe-head.
Entry Chamber	• interfaces Flow/Probe Chambers with Air Intake Chamber.
Air Intake Chr.	• fitted with filters to remove any contamination in entry air flow.
Instrumentation	• *SETRA* pressure transducers (0.5" H_2O), for Pitot probe meas. • *PSI Inc* pressure scanners (10" H_2O) for pressures in Chambers. • *PSI Inc* pressure scanners (5 psid) for pressures in Test Section. • 3-element and 1-element Hot Wire Probes. • *TSI* Constant Temperature Anemometer System, 16-channel • *B&K* Microphone probes.
Data System	• *IBM-PC-AT* with *TSI* software for hot wire data acquisition. • Unitary Wind Tunnel SWTS system. • *REP-VAX* for final analysis/compilation of data. • *MAC-II* for compilation and preparation of Data Reports.

The simulation concepts adapted for studying the flowfield characteristics of typical turbulence reduction system *(TRS)* of large wind tunnels are explained below:

BLASTANE Simulation Concept for simulating Typical TRS Systems
Boundary Layer Apparatus for Subsonic and Transonic flow Affected by Noise Environment for TRS (Turbulence Reduction System) located in Settling Chamber

ITEM	*Typical TRS of Wind Tunnels*	*BLASTANE Simulation Concepts*
Flowfield dimensioins	Large	• simulate in segments. • use several simulation configurations for each typical TRS configuration, and cross-compile the test data. • simulate stream-tubes at different points across the flow cross-section.
Pressure level	Variable.	• Atmospheric stagnation only.
Flow entering the Settling Chamber	Effect of Turning Vanes	• simulate with blockage vanes.
	Influence of Entry–Wide–Angle–Diffuser.	• simulate with blockage plates, and patched screen elements. • also use a scaled WAD model.
	Large length–scales of turbulence.	• simulate parametrically with different grids/rods/blockage–plates.
Screens	Large spacing.	• use Full Scale, at actual spacing.
	seams.	• seams separately tested.
Honeycomb	Frame-work. Hanger/Splice plates	• use Full Scale, at actual spacing. • Frame–effect separately obtained.
Heat Exchanger	Support frame.	• use Full Scale, at actual spacing. • Frame elements separately added.
	Thermal gradient.	• possibly, with heating elements.
Contraction	9:1 to 25:1	• 20:1 Ratio, scaled lengths • 9:1 ratio available.
Test Section	large dia, length.	• diameter=10" • length= 6 ft.
	large decay length	• simulate effect of settling lengths.
Exit Flow	Exit Diffuser.	• Choked (sonic) exit, influence of downstream disturbances eliminated.

These simulation concepts helped in arriving at a limited number of BLASTANE configurations, with differently located flow conditioning elements *(screens, honeycombs, heat exchanger panels)*, that needed to be tested for characterizing the flowfield. The Probe Chambers equipped with flow measuring instrumentation could be located at any desired flow station so as to measure the turbulence distribution and velocity profile at entry and exit stations of the TRS.

The instrumentation and data system developed for detailed measurements of the flow field included 3-element hot wire probes, acoustic probes, low-pressure range transducers, flow angle measuring vanes, and traversing devices (*see Figs.30, 31*).

Boundary Layer Experiments

The configuration of BLASTANE during the flow characterization tests was also suitable for some test section wall boundary layer measurements. The buried wire gage signals were analyzed in order to obtain an appreciation of the boundary layer flowfield. However, at the time of writing this report, BLASTANE apparatus was still being used for tests pertaining to simulation of the 12 FT PWT Restoration Project TRS design, and was not available for detailed boundary layer tests.

6.2 Measurements, Results and Discussion

It may be noted here that the **calibration tests and measurements** for the large number of **buried wire gages** were an important part of the experiments, and took up a considerable portion of the term of the present project. These measurements have been discussed in an earlier section of this report, and will not be repeated here.

The next phase in the measurements was the one relating to characterization of the turbulence field in large wind tunnels. As mentioned earlier in this report, the test program pertaining to the present project was merged with the simulation tests aimed at providing a database on the design of the Turbulence Reduction System *(TRS)* of the 12 FT PWT Restoration project. The test results pertaining to the present project are presented below:

Results from flow-characterization tests:

- Test Section turbulence levels were in the range of 0.03% to 0.06% for contraction-entry turbulence levels of up to about 1.0%. For higher entry turbulence levels, the test section turbulence levels were higher. *(see Fig.32)*
  (Note that the contraction ratio is 20:1)

- Turbulence level in the test section remained invariant from entry to the 36" station *(which was the last measurement station)* along the length of the test section.

- Turbulence reduction ratio, *i.e., the ratio of test section turbulence to the contraction entry turbulence*, matched the inverse of contraction ratio only for entry turbulence levels higher than 0.8%, but did not match for lower entry turbulence levels *(see Fig.32)*

- For a given turbulence level at entry to contraction, the test section turbulence was higher for higher Mach numbers, perhaps because of compressibility effects *(see Fig.32)*

- A 3-element hot wire probe, containing 50 *micron* fiber-film elements, was used in the test section to measure the different components of turbulence. These measurements did not compare well with the single element hot wire probes containing 5 *micron* tungsten wires. It was suspected that the 3-element probe, because of the larger sensor diameter, would not give proper measurements for flow speeds larger than *Mach* 0.3. 3-element probes with slender sensors were not readily available.
  It was possible to confirm that, for lower flow speeds, the test section turbulence field was essentially isotropic.

- Test Section wall pressure fluctuation measurements were made with flush-mounted pressure transducers. For the case of low turbulence at entry to contraction, which represented the baseline flow condition for boundary layer studies, the pressure fluctuations were in the range 0.3% to 0.5% along the length of the test section.
  It may be noted that the exit flow from the test section is choked by a flow control plug in BLASTANE, entirely eliminating any influence of flow noise downstream of the diffuser. Higher acoustic noise levels are to be achieved in BLASTANE by introducing an electrically driven speaker at the entry to the Contraction or Settling Chamber.

Results from Baseline boundary layer measurements:

- It was confirmed that the desired baseline Test Section flow condition of very low flow unsteadiness level was achievable with 5 screens at the entry to the Contraction. Measurements for that configuration showed that the baseline turbulence was in the range *0.03 to 0.08 %*, and pressure fluctuations were in the range *0.07 to 0.15 %*, depending on the Mach number *(higher levels for higher Mach nos.)*.

- For the case of baseline flow condition, *i.e.*, low turbulence low acoustic noise level in the freestream, signals from buried wire gages mounted at several wall stations were analyzed with the respective calibration data. The gages appeared to perform satisfactorily.

7 Concluding Remarks

The progress made with respect to the objectives of the Cooperative Agreement are summarized below:

- Existing research publications were reviewed extensively, to finally determine that the many theoretical methods that exist for predicting the effects of flow unsteadiness components on boundary layer transition may be adequate for low subsonic flow speeds, but are not reliable for high subsonic flow speeds, primarily because of the effects of compressibility.

- The existing database on boundary layer transition at high flow speeds was reviewed in an effort to properly isolate the individual effects of Mach number, acoustic pressure fluctuations, and freestream turbulence. A systematic procedure, inspired by the well established correlations for incompressible boundary layers and the findings of flight experiments, was evolved to carefully separate the effects of the individual flow unsteadiness components. New correlation laws were established for the individual effects *(see Chapter-2)*

- The Experimental Apparatus, namely the *Boundary Layer Apparatus for Subsonic and Transonic flow Affected by Noise Environment (BLASTANE)*, was fully developed to undertake a testing program for collecting detailed data on the effects of the individual flow unsteadiness variables. Acoustic noise levels and turbulence levels in this apparatus were reduced to very low levels in order to acquire base-line data for very low mass flux fluctuations and pressure fluctuations *(the two most important parameters in the flow unsteadiness field)*.

- Baseline Test Section flow conditions were found to be of very low turbulence *(0.03 to 0.08 %)*, and very low pressure fluctuations *(0.07 to 0.15 %)*, depending on the Mach number *(higher levels for higher Mach nos.)*.

- Special instrumentation, *primarily the buried wire gage technique*, was developed for obtaining reliable indications of boundary layer transition, and for measuring wall flow skin friction distribution. A large number of gages, *a total of about 120*, were built into the instrument plugs of the BLASTANE test section, so that the gages could be used for obtaining wall-flow properties simultaneously at a series of stations along the length of the boundary layer flowfield. All the gages were calibrated fully in a standard pipe-flow, and made ready for detailed boundary layer measurements.

- As a part of the gage calibration data reduction effort, a new method was developed for analyzing compressible pipe flow. This analysis made it possible to correctly derive wall flow friction values from wall pressure distribution measurements for high subsonic flow speeds. The new method consisted of applying an integral technique to transform the basic compressible flow equations into a set of integral governing equations, and then applying the knowledge of flat plate compressible boundary layers to provide closure to those governing equations. This method was validated by performing a special series of tests on pipe flow, with centerline Mach numbers ranging from low subsonic to almost sonic, and evaluating the detailed wall pressure measurements *(see section 4.4)*.

- Buried Wire Gages were mounted in the test section and operated to obtain data at different freestream conditions. The gages appeared to be performing satisfactorily.

- It may be noted that the apparatus and instrumentation were brought to a status at which boundary layer transition data acquisition tests could be commenced, but the apparatus was to be used on another higher priority project, namely the 12 FT PWT Restoration Turbulence Reduction System Design Project. It was possible to combine the flow-characterization tests of the present project with the higher priority project, and obtain a good database. But, the boundary layer transition tests remained at a lower priority all the way up to the writing of this final report.

- It is recommended that a series of data generation tests for boundary layer transition phenomena be taken up in a future research project, with the instrumentation developed in the present project, so that a first-of-the-kind database may be made available in that subject area.

8 List of Publications

1. Murthy, S.V. and Steinle, F.W., "On Boundary Layer Transition in High Subsonic and Transonic Flow under the Influence of Acoustic Disturbances and Free-stream Turbulence," *AIAA Paper 85-0082, Reno, NV.*, Jan. 1985.

2. Murthy, S.V. and Steinle, F.W., "Effects of Compressibility and Free-stream Turbulence on Boundary Layer Transition in High Subsonic and Transonic Flows," *AIAA Paper 86-0764, West Palm Beach, Fl.*, Mar. 1986.

3. "Documentation pertaining to design and safety aspects of BLASTANE (*Boundary Layer Apparatus for Subsonic and Transonic flow Affected by Noise Environment)*— Safe Operating Procedure ('SOP', Document No. A-327C-8401-SD4, Oct. 1986), System Safety Hazard Action Status Reports (Vol.1 on Preliminary Hazard Analysis Items, and Vol.2 on Operational Hazard Analysis Items, Document Nos. A-327C-8401-SD1 and SD-2, Oct. 1986), Integrated Systems Test plan ('IST—plan', Document No. A-327C-8401-SD5, Oct. 1986), Completion of the Integrated Systems Test for BLASTANE ('IST—completion tests, Document No. A-327C-8401-SD5, Feb. 19, 1987), Aerodynamic Facilities Branch (Code *RAF*), *Engineering Documentation Center, NASA Ames Research Center, Moffett Field, CA*, 1986–87.

4. Murthy, S.V. and Steinle, F.W., "Calibration Data for Buried Wire Gages to be used in BLASTANE Experiments", Calibration Data Report, (Internal Report) prepared under Co-op Agreement No. NCC 2-357, *Aerodynamic Facilities Branch, NASA Ames Research Center*, Oct. 1986.

5. Murthy, S.V. and Steinle, F.W., "Development and Calibration of Buried Wire Gages for Wall Shear Stress Measurements in Fluid Flow", accepted for presentation as Paper No. 88–2022 at the *AIAA 15th Aerodynamic Testing Conference, San Diego, CA*, May 18–20, 1988.

6. Murthy, S.V., K. Gee, and Steinle, F.W., "Compressibility Effects on Flow Friction in a Fully Developed Pipe Flow", accepted for presentation as Paper No. 57 at the *First National Fluid Dynamics Congress, Cincinnati, OH*, July 25–28, 1988.

7. "Simulation Studies of Flow Quality Characteristics and Control in a Closed-loop Wind Tunnel Circuit", — Documentation pertaining to (i) use of BLASTANE Apparatus for studies of flow characteristics emerging from commonly used flow conditioning elements, (ii) Proposed additions to the Apparatus for acquiring test data on flow conditioning elements, (iii) Aerodynamic loads for Modifications of BLASTANE, etc., by S.V. Murthy and F.W. Steinle, submitted to *Aerodynamics Division — 12 FT PWT Restoration Project, NASA Ames Research Center, Moffett Field, CA*, Jan—Mar. 1988

SOURCES OF FLOW UNSTEADINESS : FREESTREAM TURBULENCE
PRESSURE FLUCTUATIONS
TEMPERATURE SPOTTINESS

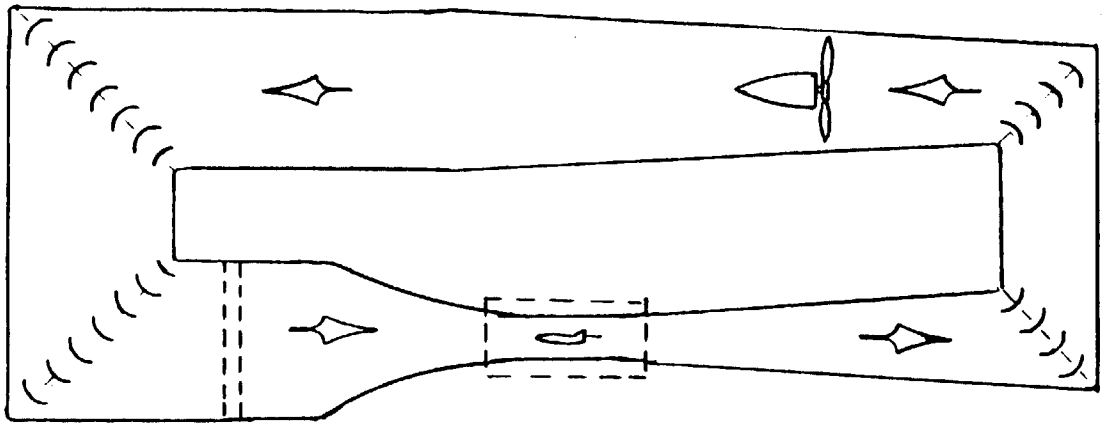

WIND TUNNELS

FAN ROTATION
FLOW TURNING AT BENDS
WALL BOUNDARY LAYER
WALL GEOMETRY
MODEL SUPPORT

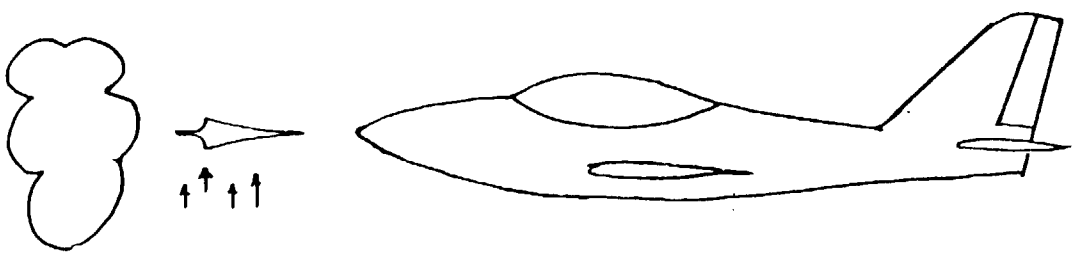

FLIGHT

GUSTY WIND
TEMPERATURE GRADIENTS
CLEAR AIR TURBULENCE
OTHER PART OF AIRCRAFT

Figure 1. WIND TUNNEL AND FLIGHT ENVIRONMENT

BACKGROUND

TWO DIMENSIONAL FLOW AROUND AN AIRCRAFT WING SECTION

BOUNDARY LAYER IS THE THIN RETARDED FLOW LAYER NEXT TO THE WALL, CAUSED BY VISCOSITY

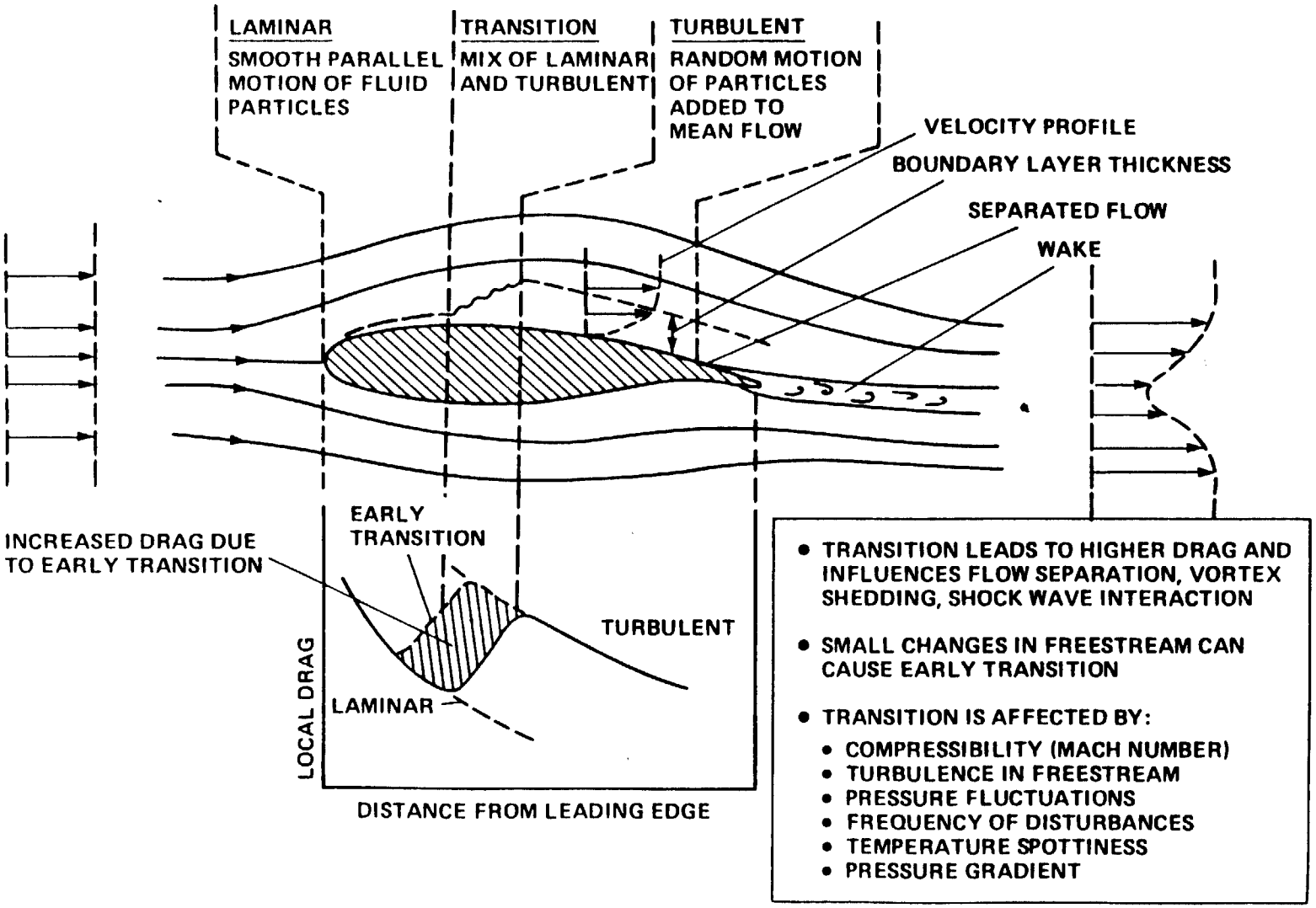

Figure 2. FLOW-FIELD AROUND AN AIRCRAFT WING SECTION

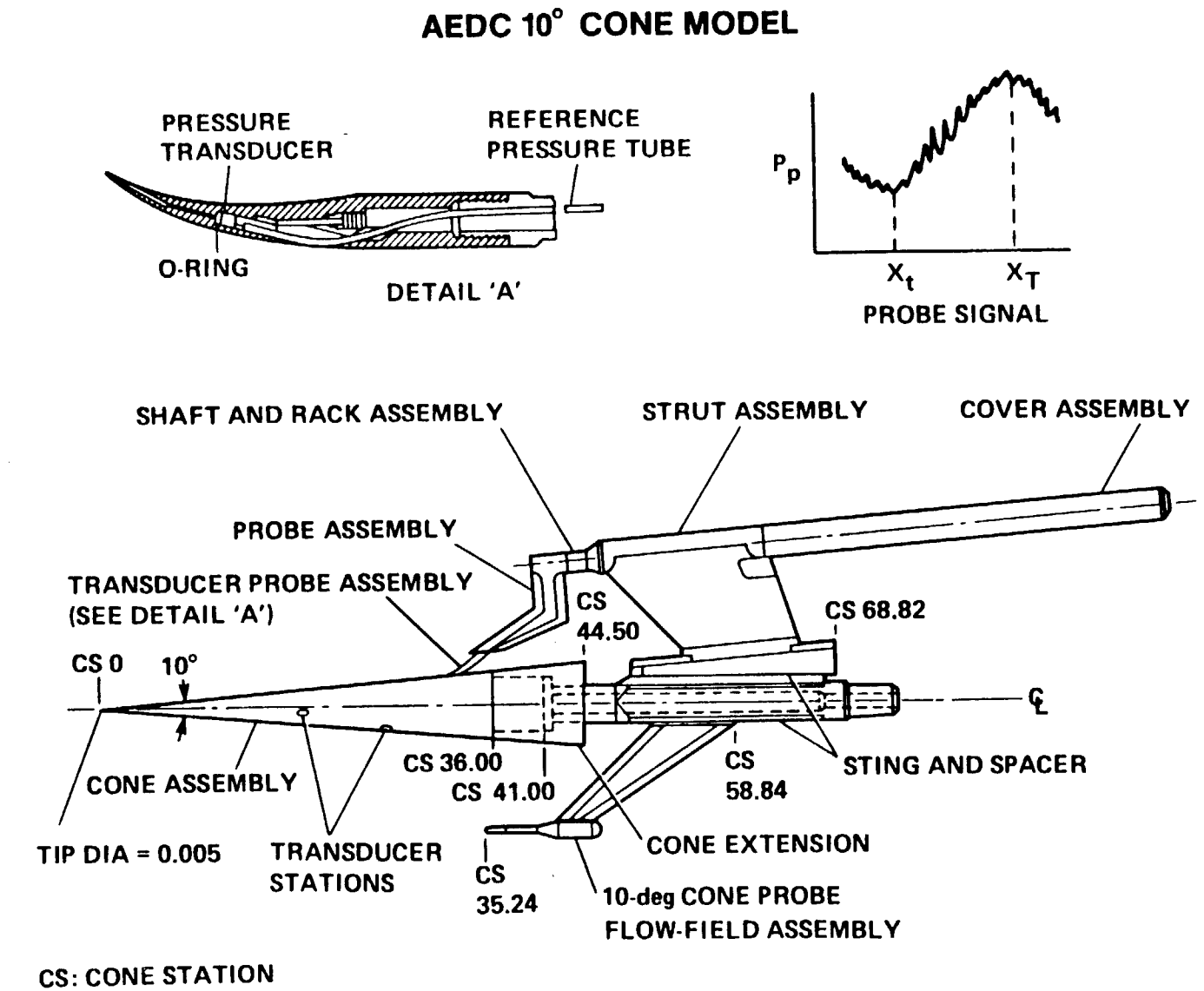

Figure 3. THE 'STANDARD' AEDC 10-DEGREE CONE

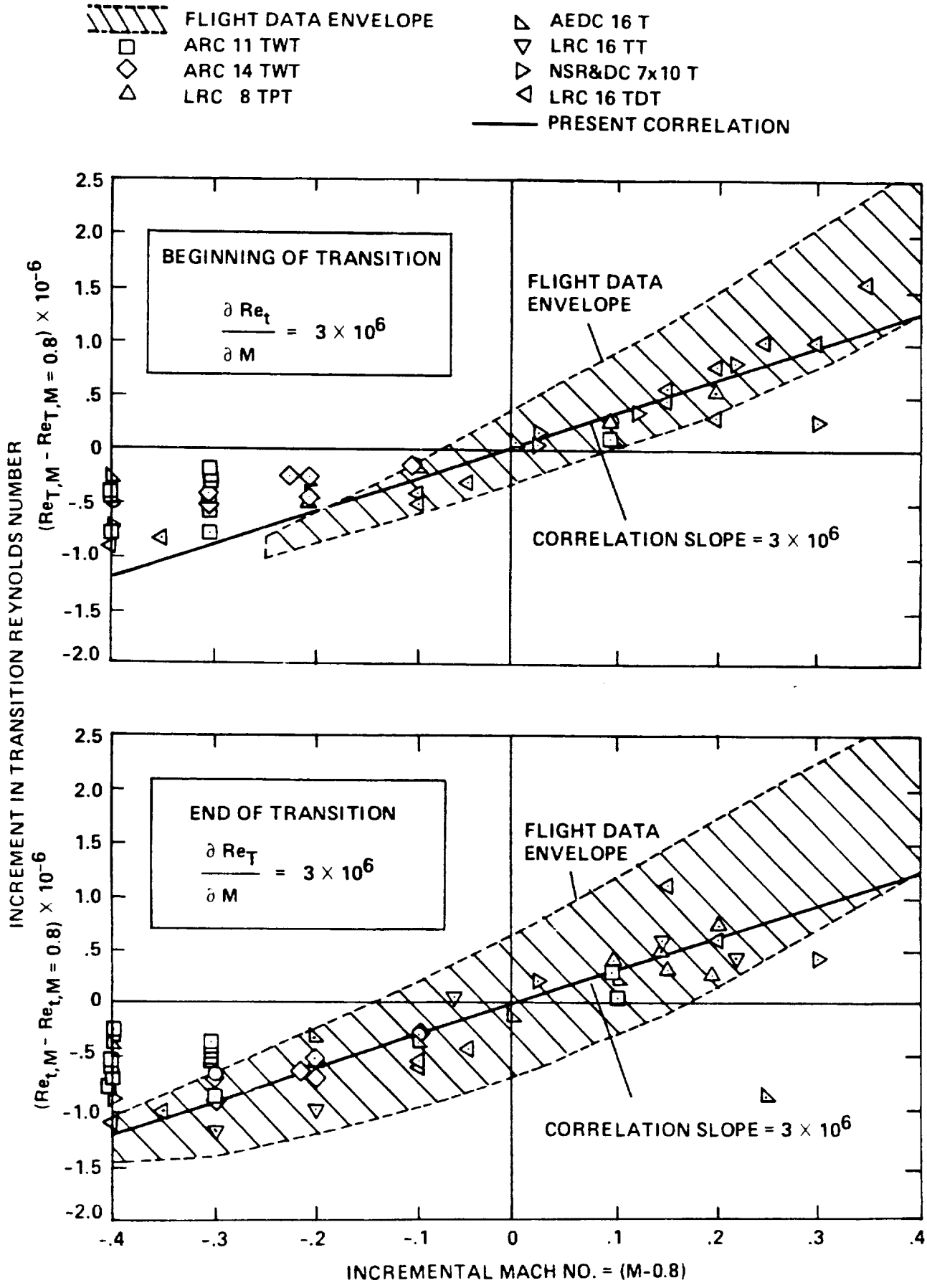

Figure 4. TRANSITION REYNOLDS NUMBER AS A FUNCTION OF MACH NUMBER

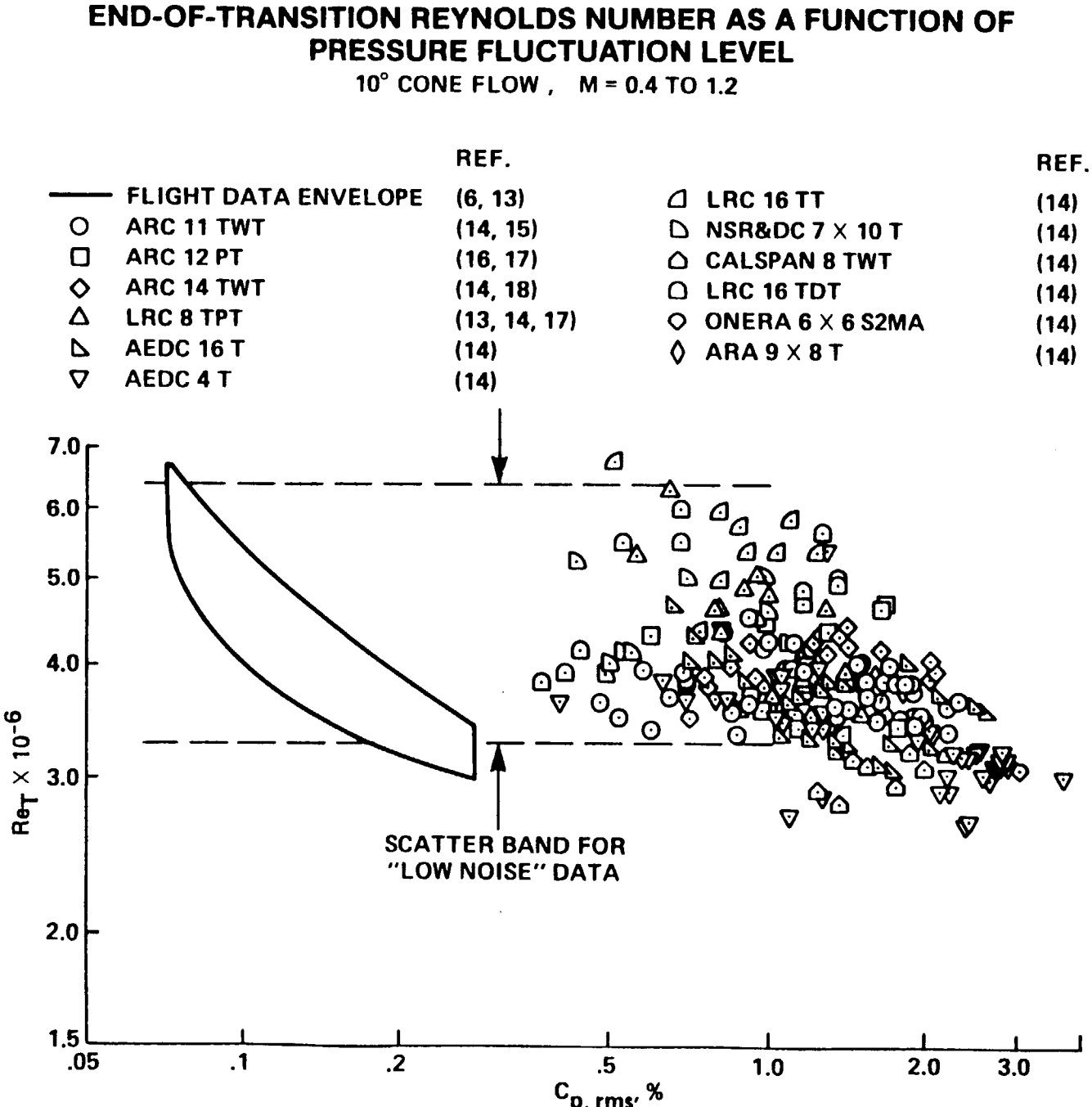

Figure 5. TRANSITION REYNOLDS NUMBER AS A FUNCTION OF PRESSURE FLUCTUATION LEVEL

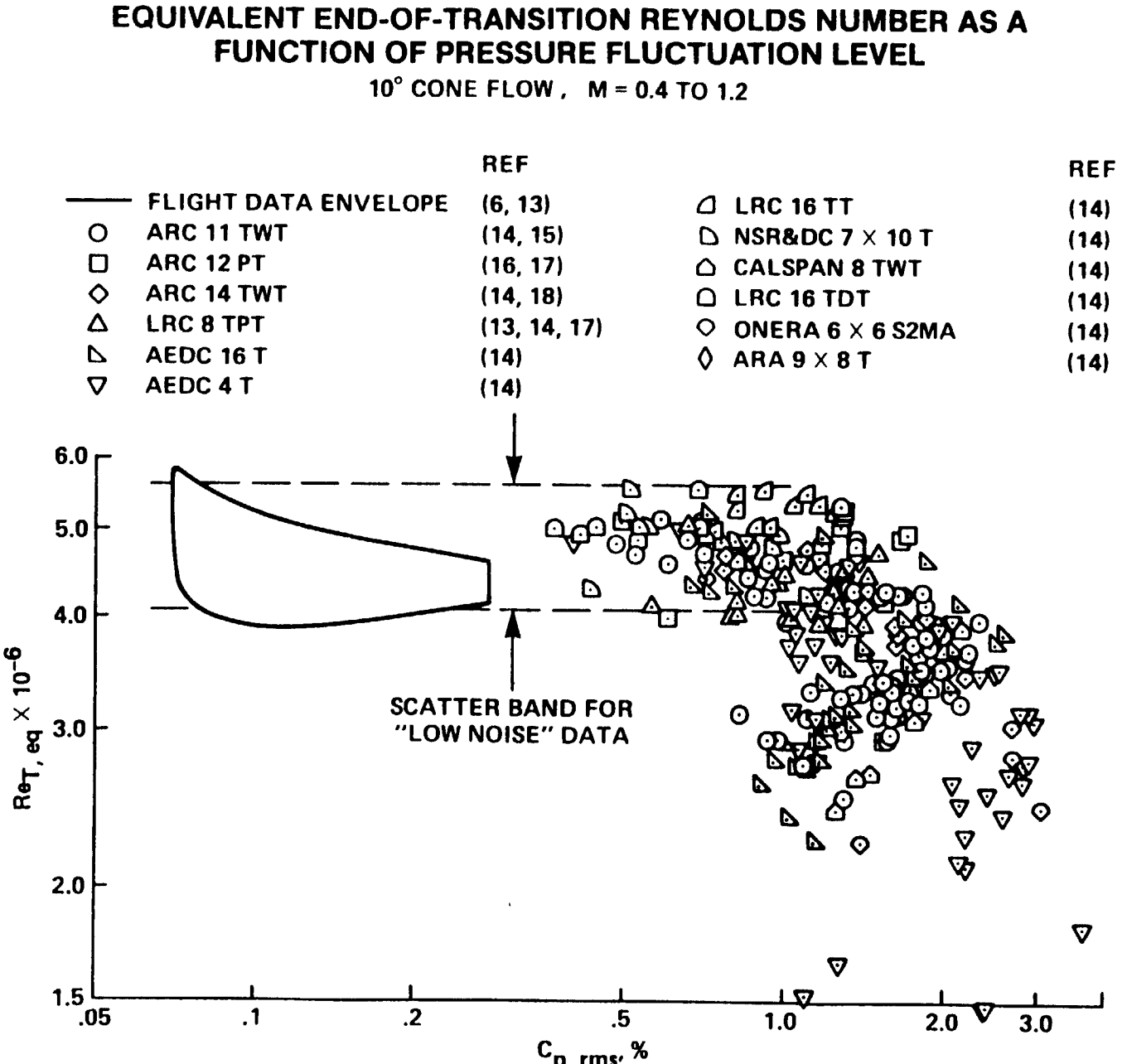

Figure 6. EQUIVALENT TRANSITION REYNOLDS NUMBER AS A FUNCTION OF PRESSURE FLUCTUATION LEVEL

RESULTS

EFFECT OF FREESTREAM TURBULENCE ON BOUNDARY LAYER TRANSITION

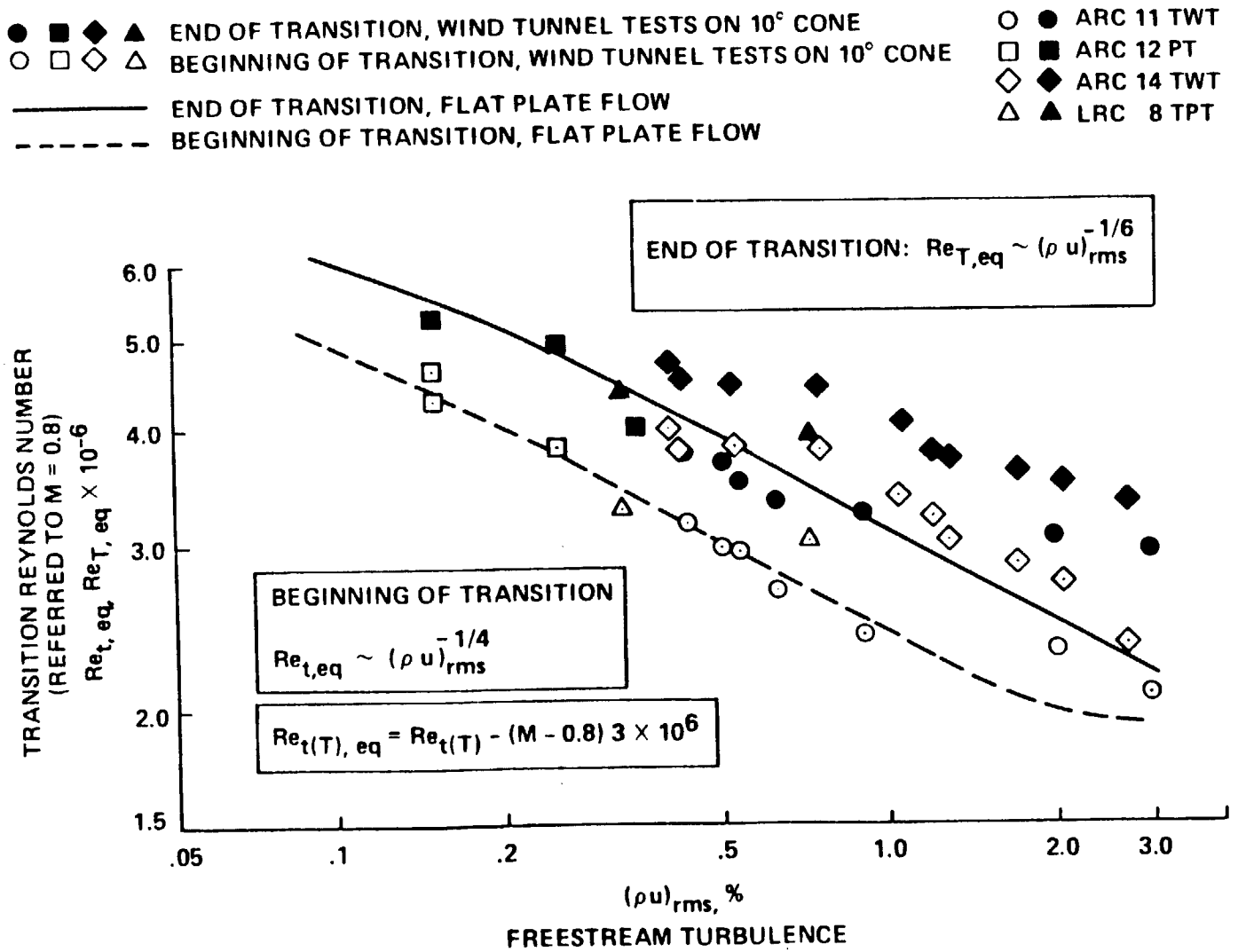

Figure 7. EQUIVALENT TRANSITION REYNOLDS NUMBER AS A FUNCTION OF FREESTREAM TURBULENCE

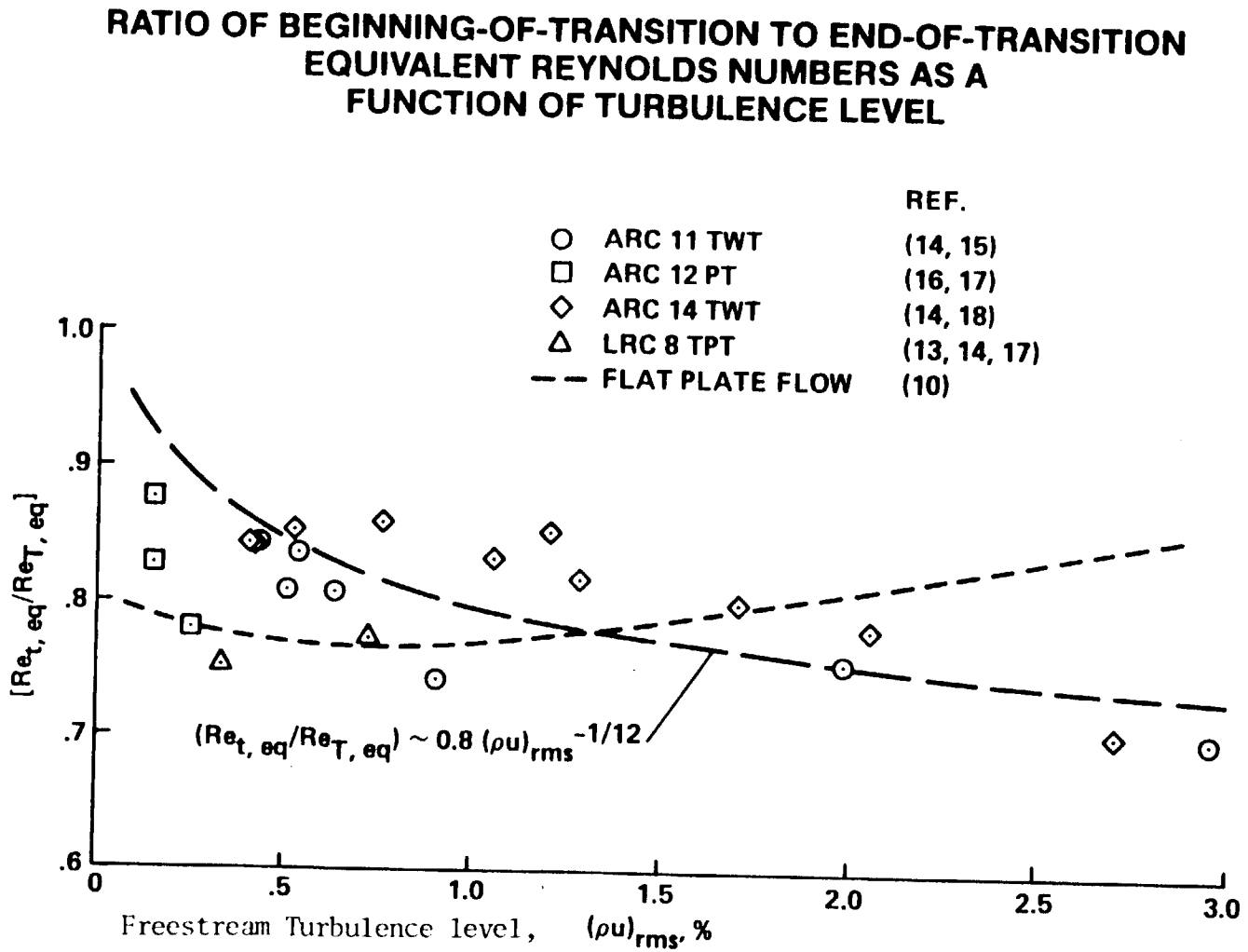

Figure 8. RATIO OF BEGINNING TO END OF TRANSITION REYNOLDS NUMBER AS A FUNCTION OF TURBULENCE

BOUNDARY LAYER APPARATUS FOR SUBSONIC AND TRANSONIC FLOW AFFECTED BY NOISE ENVIRONMENT ('BLASTANE')

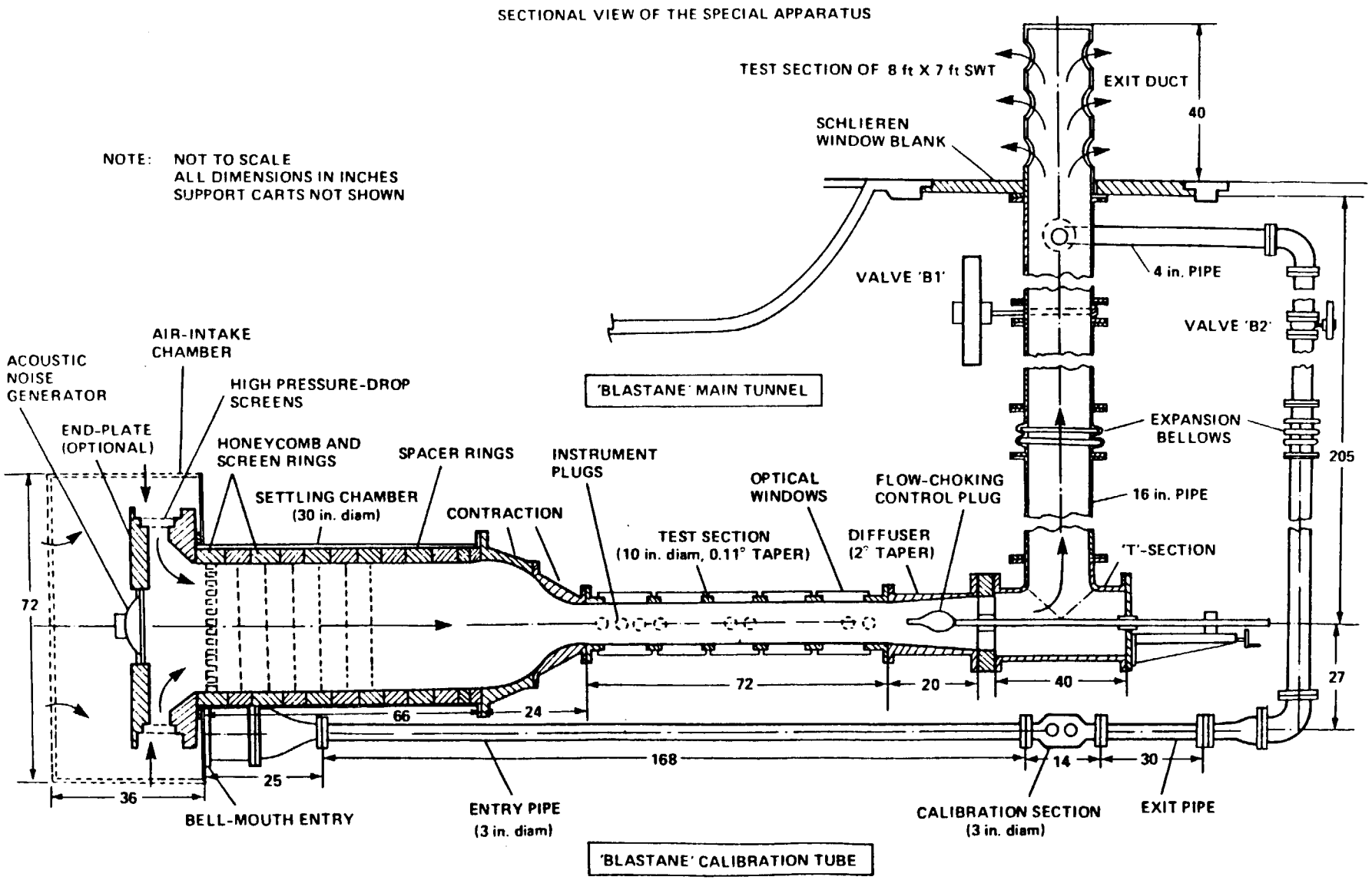

Figure 9. 'BLASTANE' APPARATUS - SECTIONAL VIEW

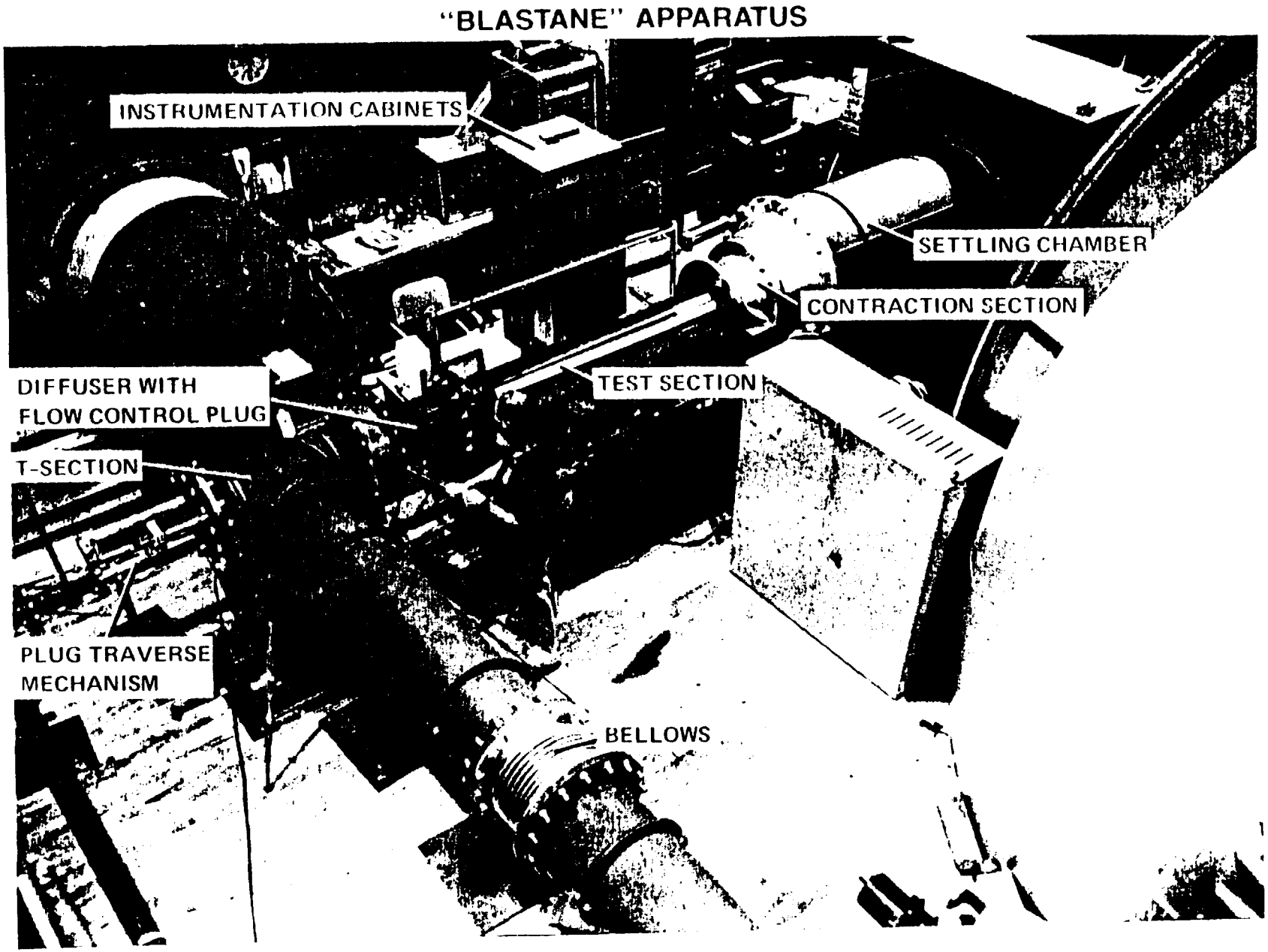

Figure 10. "BLASTANE" APPARATUS - GENERAL VIEW

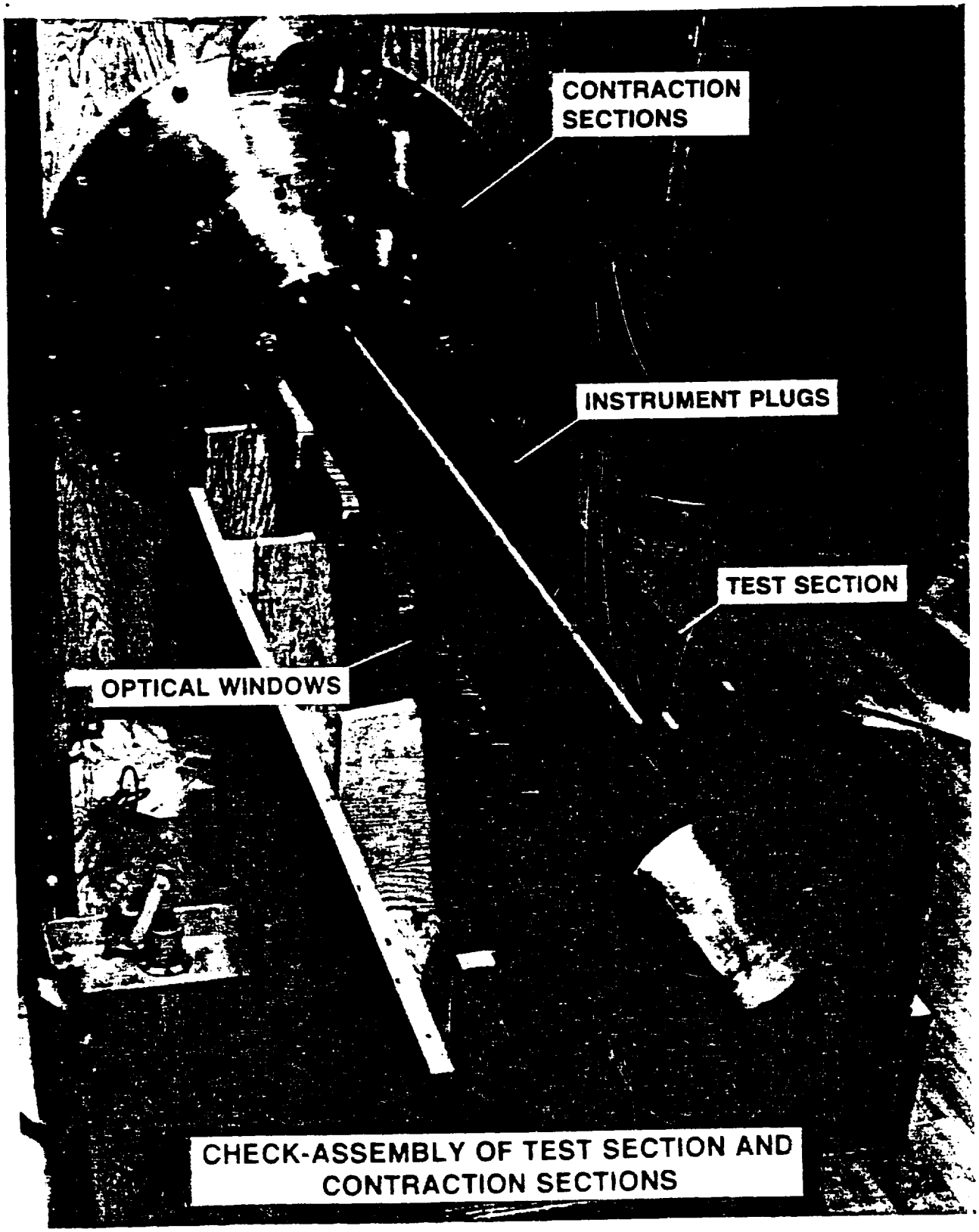

Figure 11. "BLASTANE" APPARATUS- TEST SECTION

BLOCK SCHEMATIC FOR INSTRUMENTATION AND DATA SYSTEM OF BOUNDARY LAYER APPARATUS FOR SUBSONIC AND TRANSONIC FLOW AFFECTED BY NOISE ENVIRONMENT

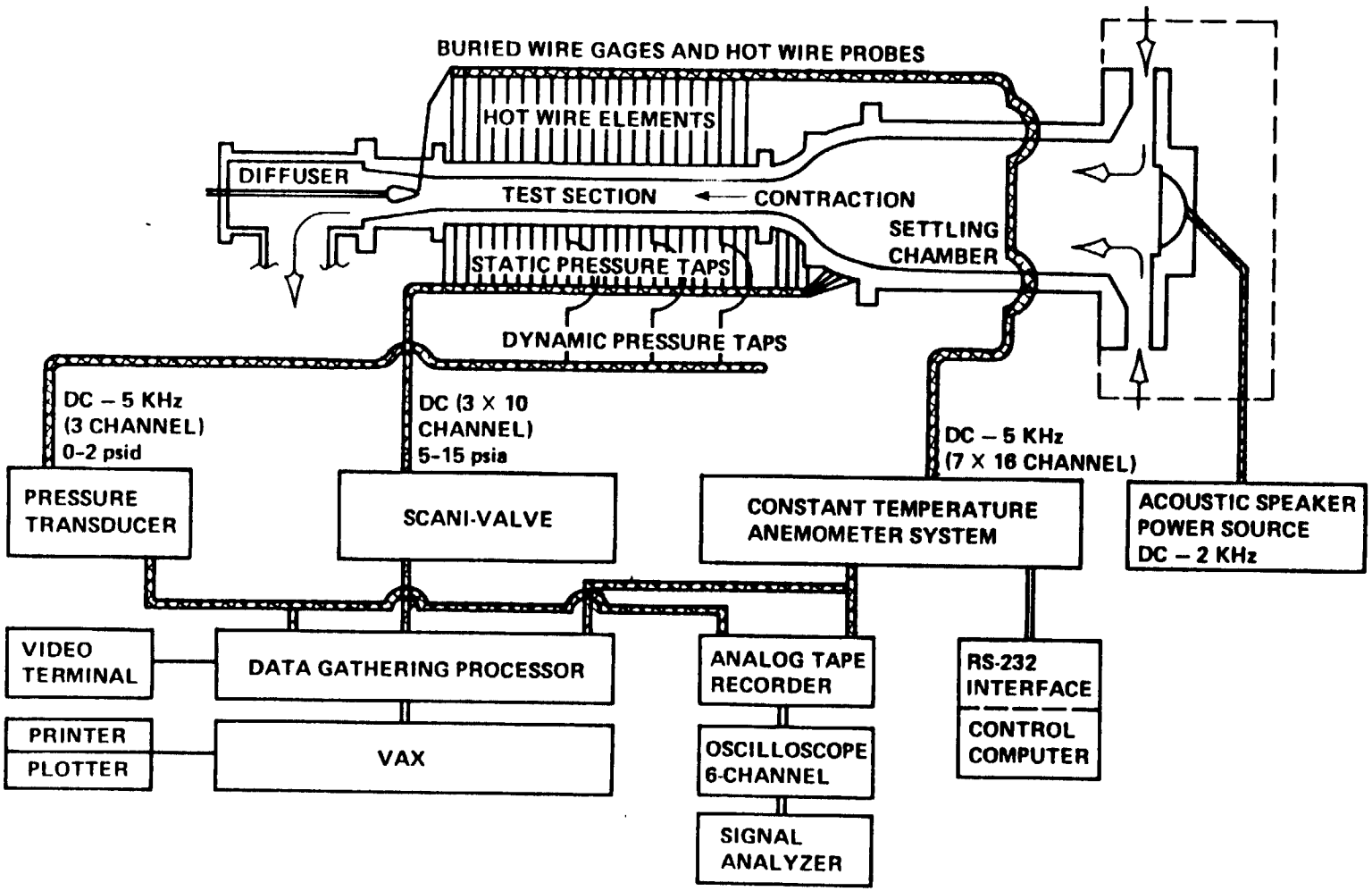

MURTHY

Figure 12. SCHEMATIC OF INSTRUMENTATION IN "BLASTANE" APPARATUS

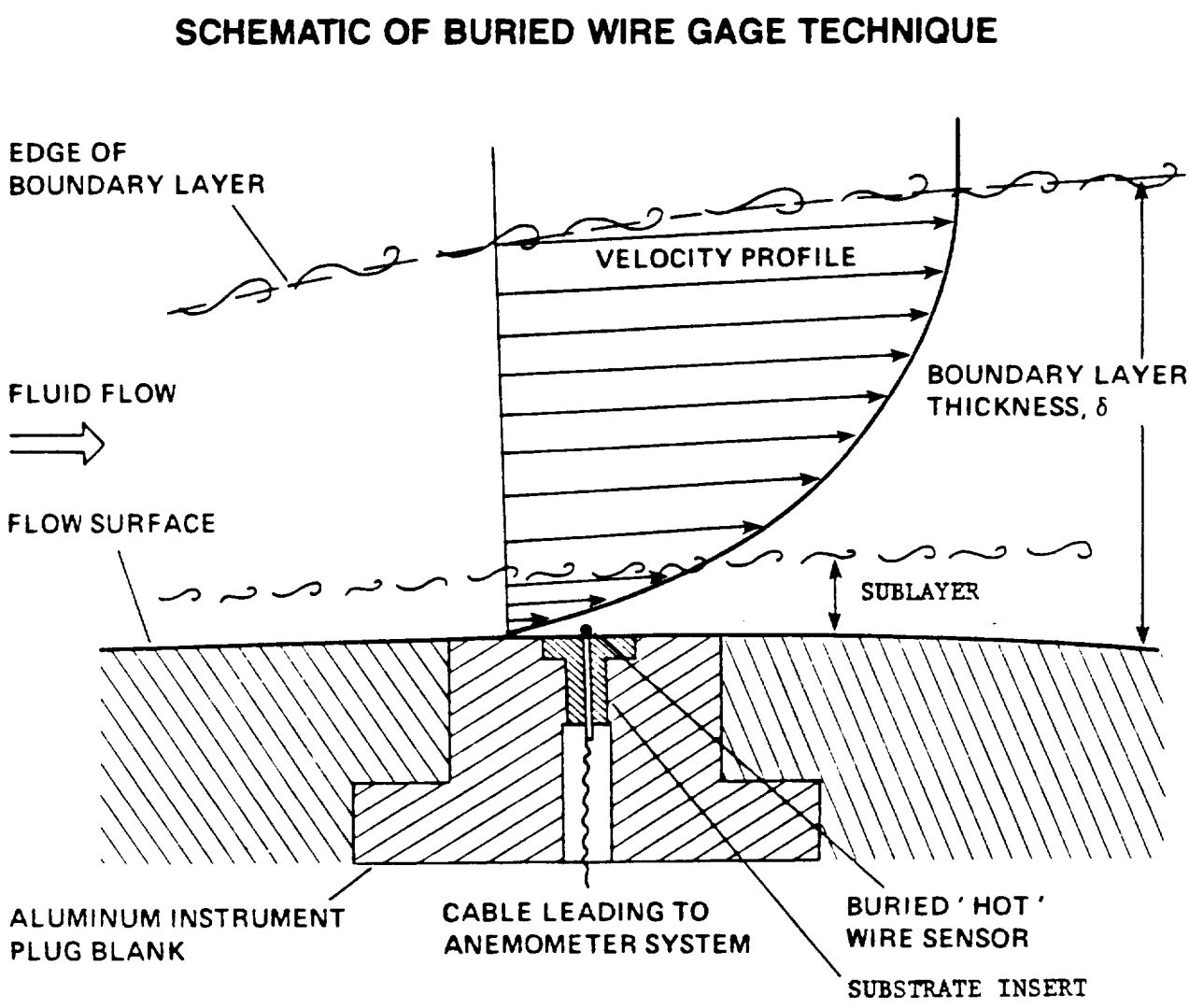

Figure 13. SCHEMATIC OF BURIED WIRE GAGE TECHNIQUE

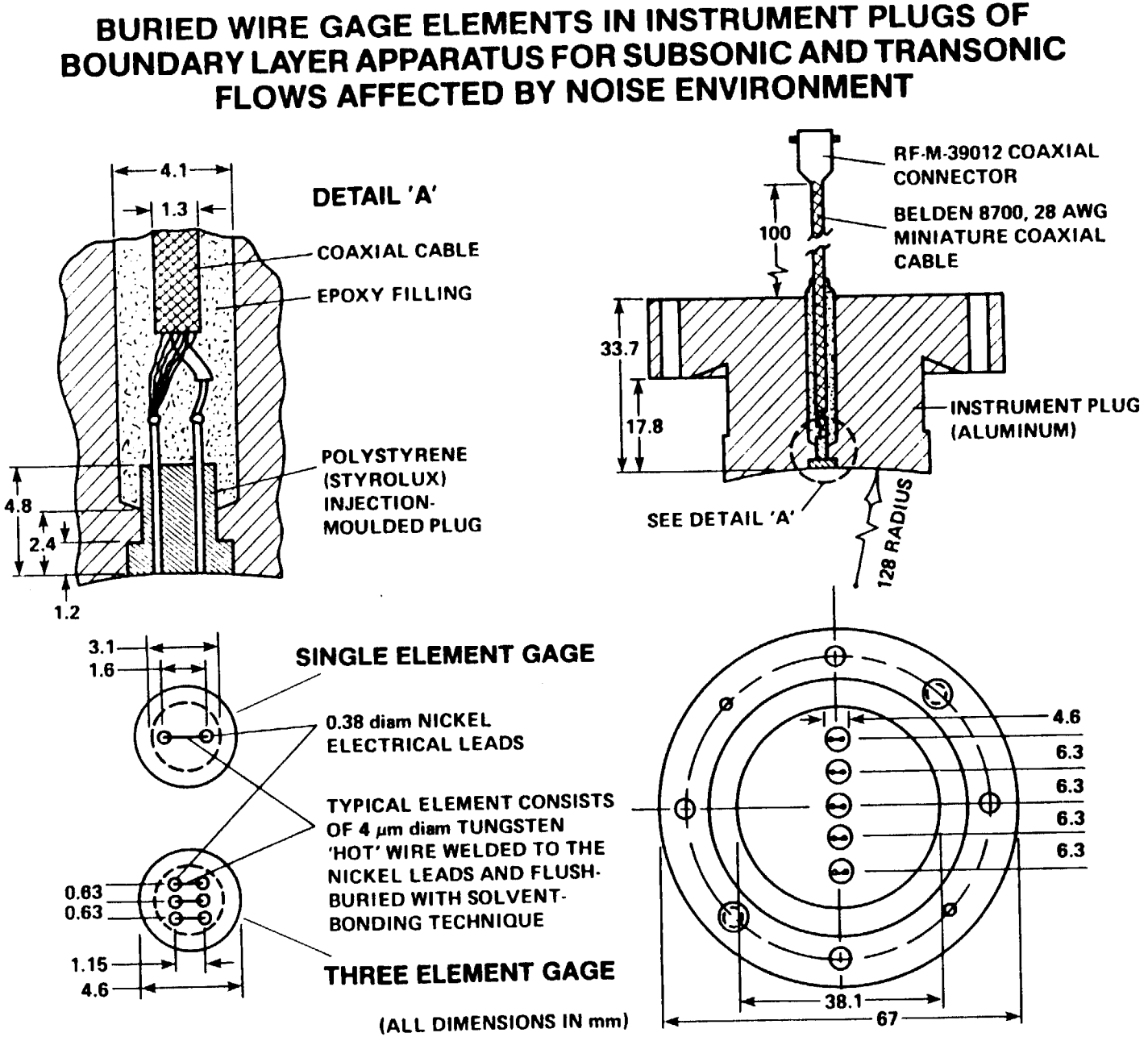

Figure 14. BURIED WIRE GAGE ELEMENTS IN INSTRUMENT PLUG BLANK. - SECTIONAL VIEW

INSTRUMENT PLUG BLANK WITH BURIED WIRE GAGES

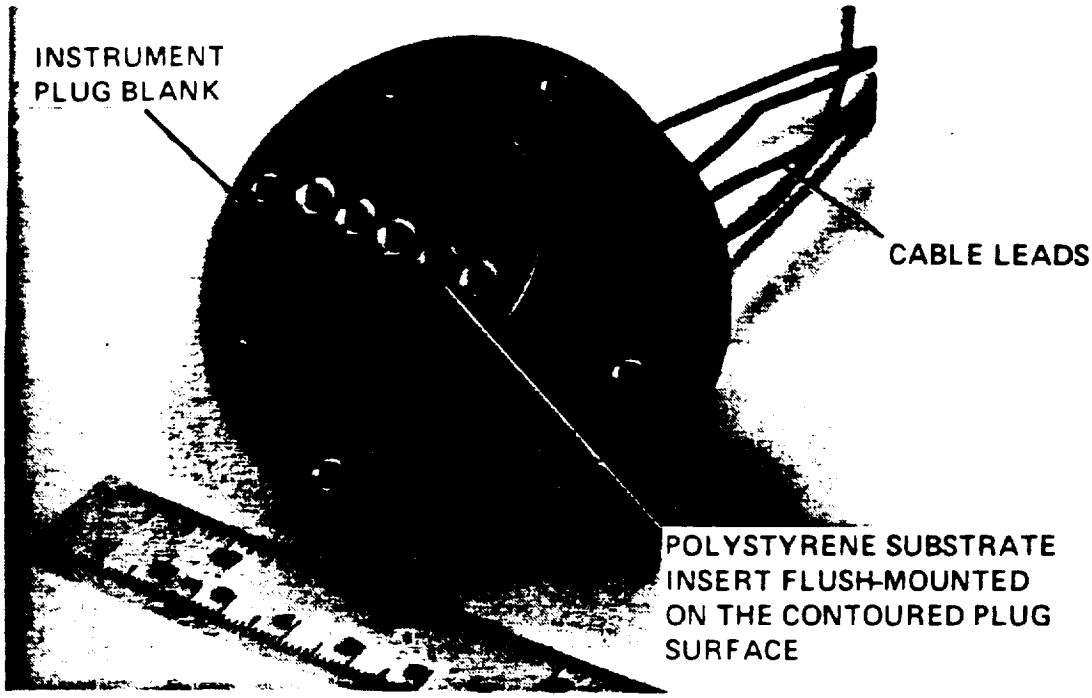

PLUG BLANK WITH 5 GAGES

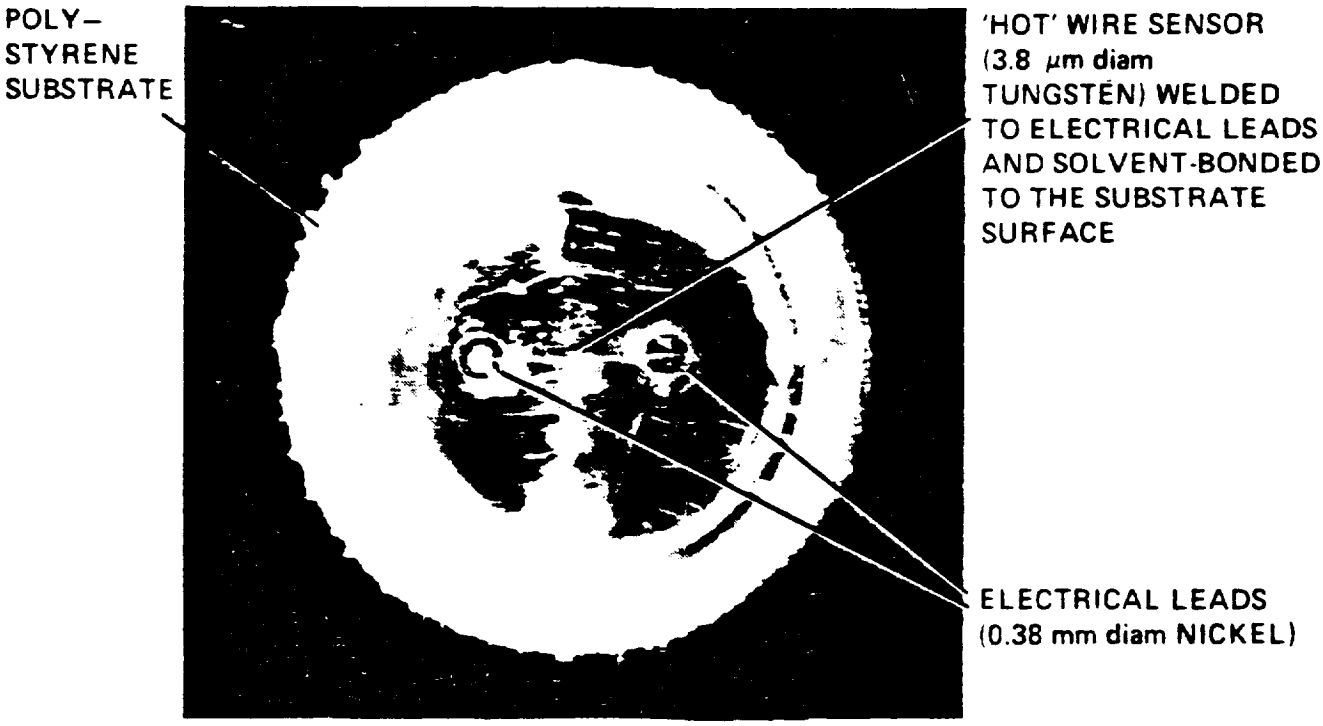

MAGNIFIED VIEW OF A BURIED WIRE GAGE

Figure 15. INSTRUMENT PLUG BLANK WITH BURIED WIRE GAGES.

ANEMOMETER BRIDGE AND TEST SIGNAL CIRCUIT

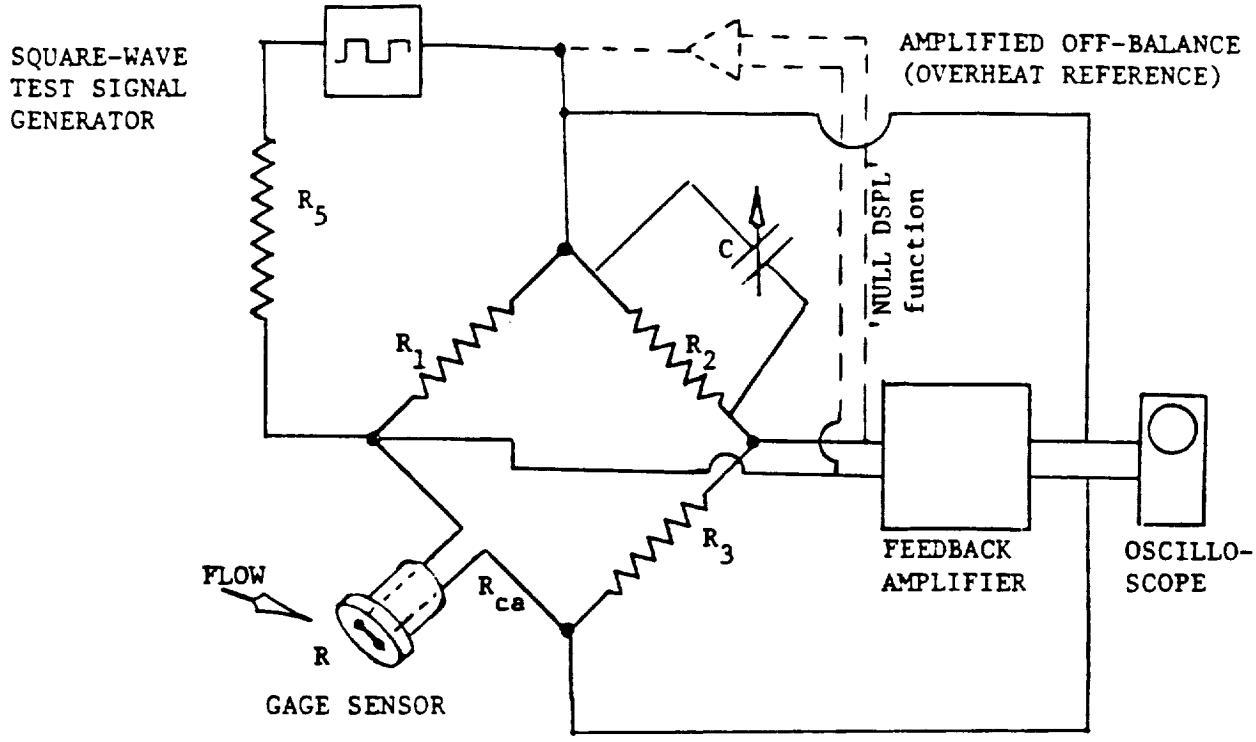

(a) ANEMOMETER BRIDGE CIRCUIT AND FEEDBACK SYSTEM

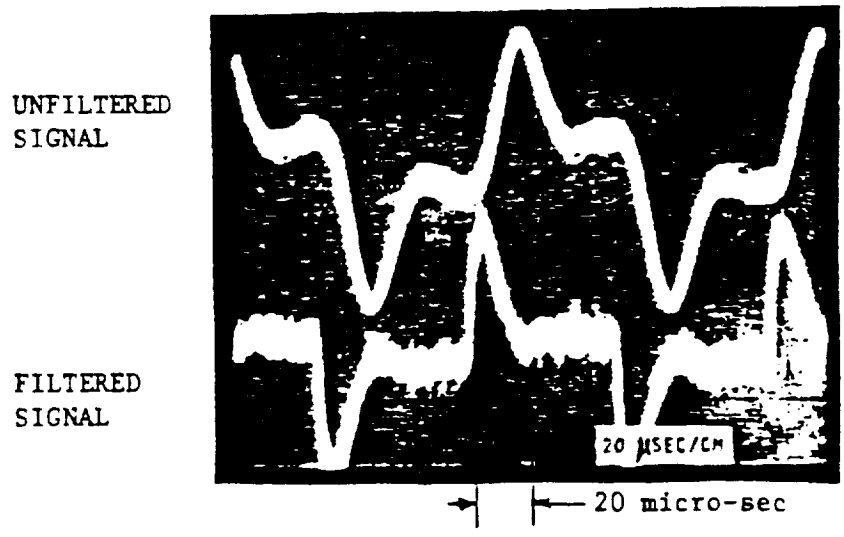

(b) OSCILLOSCOPE TRACE OF SQUARE WAVE TEST SIGNAL RESPONSE

Figure 16. ANEMOMETER BRIDGE AND TEST SIGNAL CIRCUIT

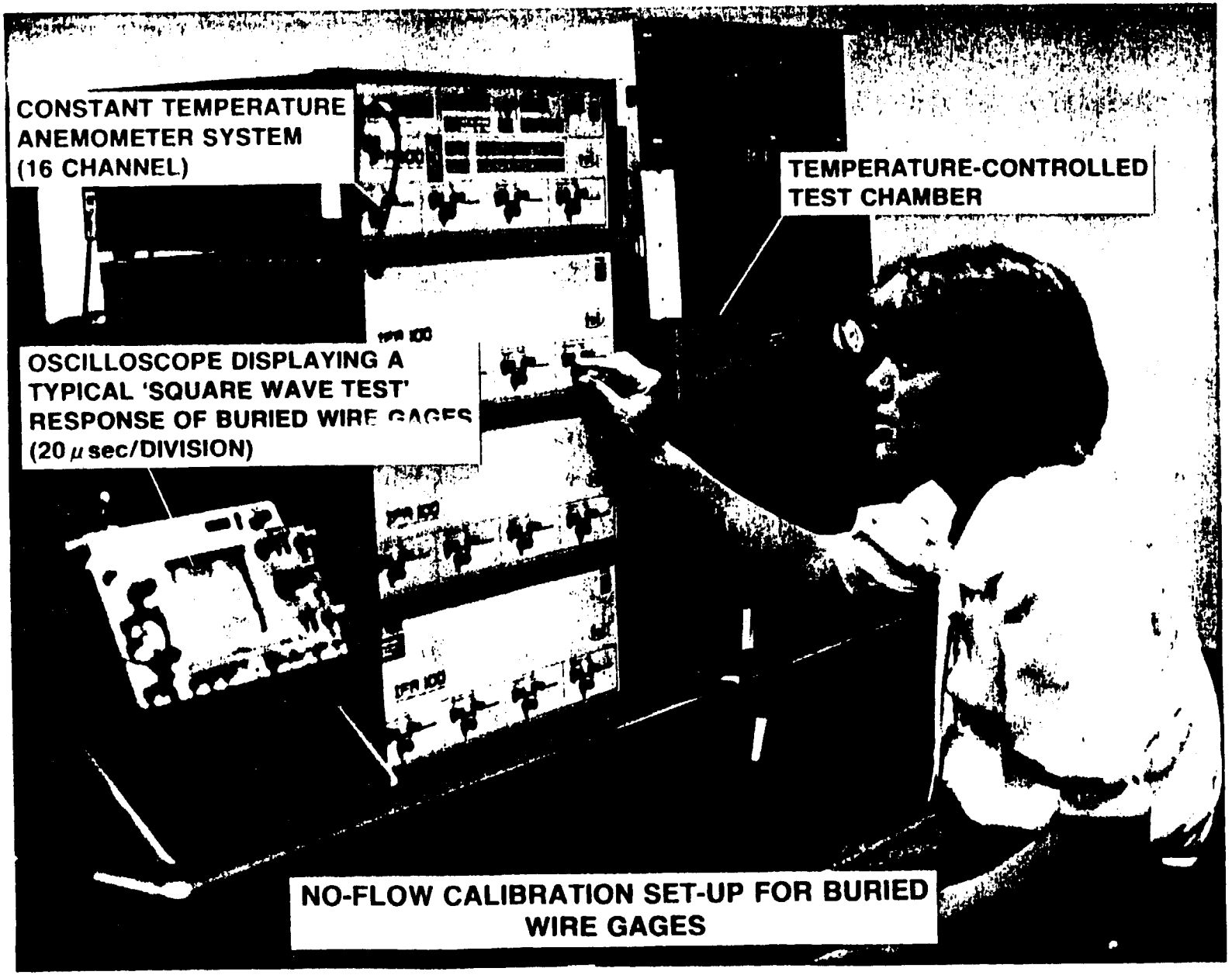

Figure 17. CONDUCTION LOSS FACTOR CALIBRATION SET-UP

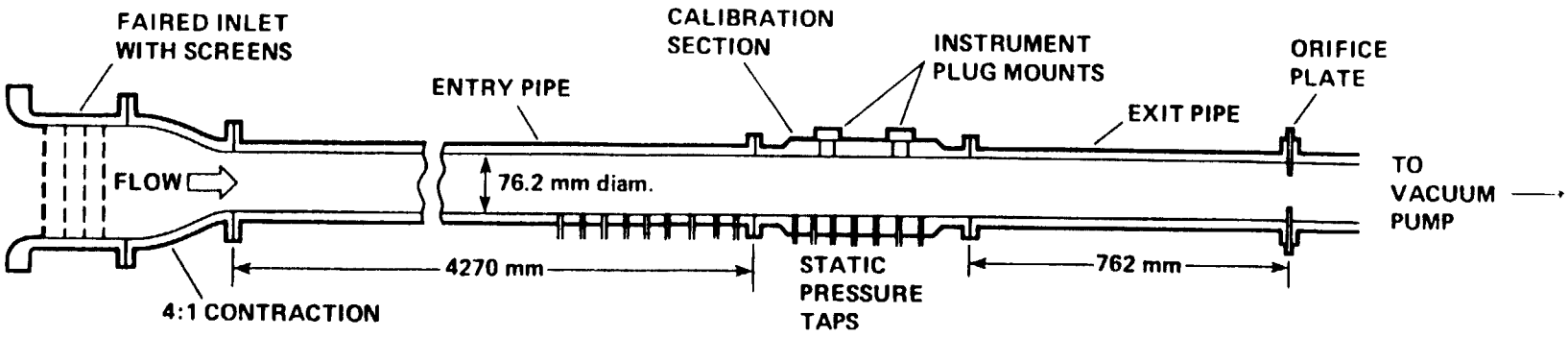

SCHEMATIC OF THE CALIBRATION TUBE APPARATUS

'TSI' ANEMOMETER SYSTEM

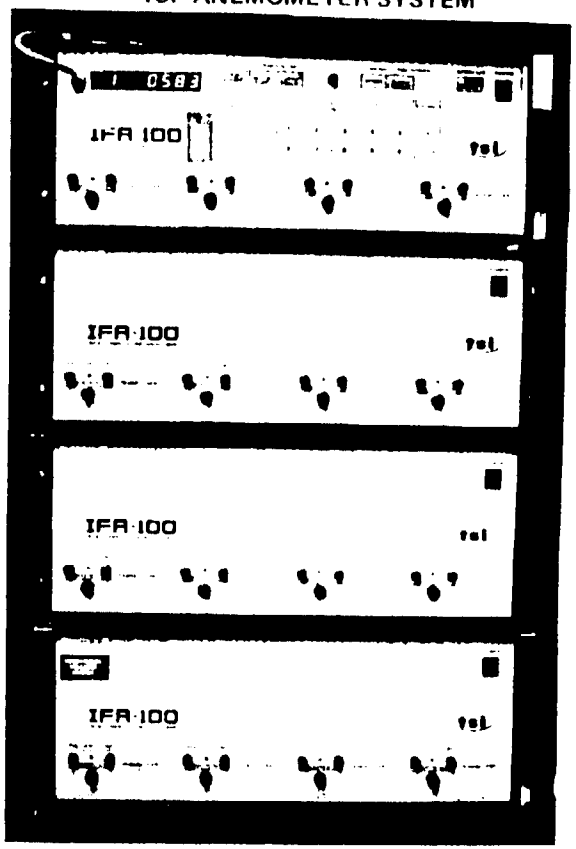

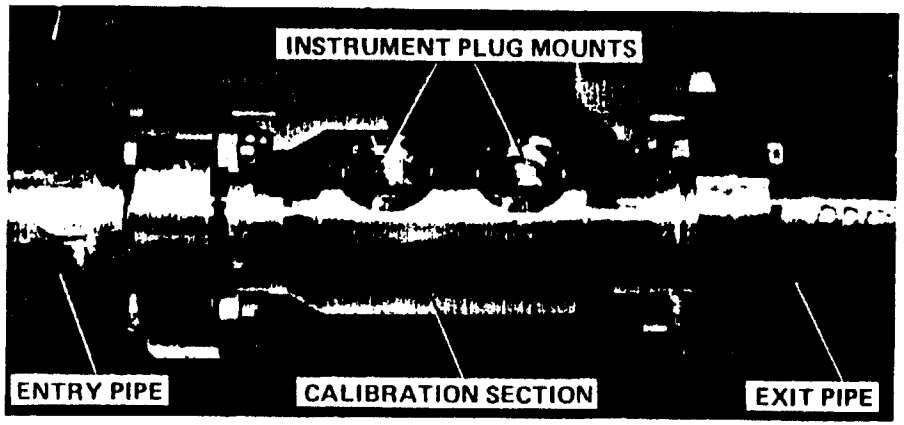

PHOTOGRAPH OF CALIBRATION SECTION

Figure 18. PIPE FLOW APPARATUS FOR EQUIVALENT LENGTH FACTOR CALIBRATION OF GAGES

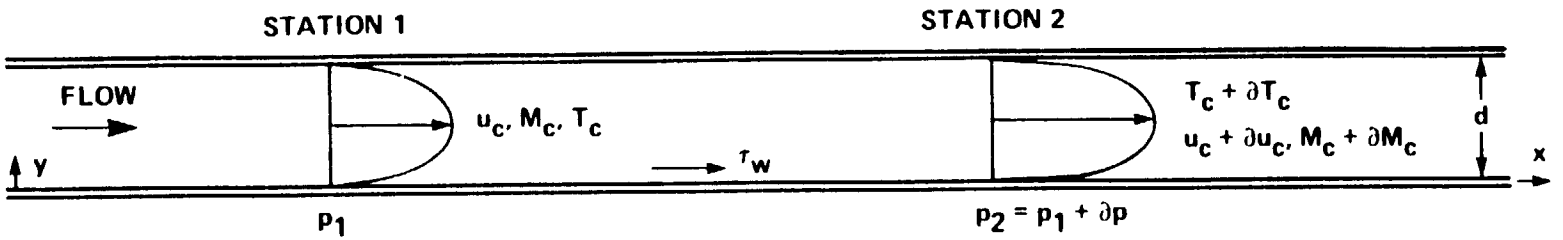

SCHEMATIC OF COMPRESSIBLE FLOW IN A PIPE

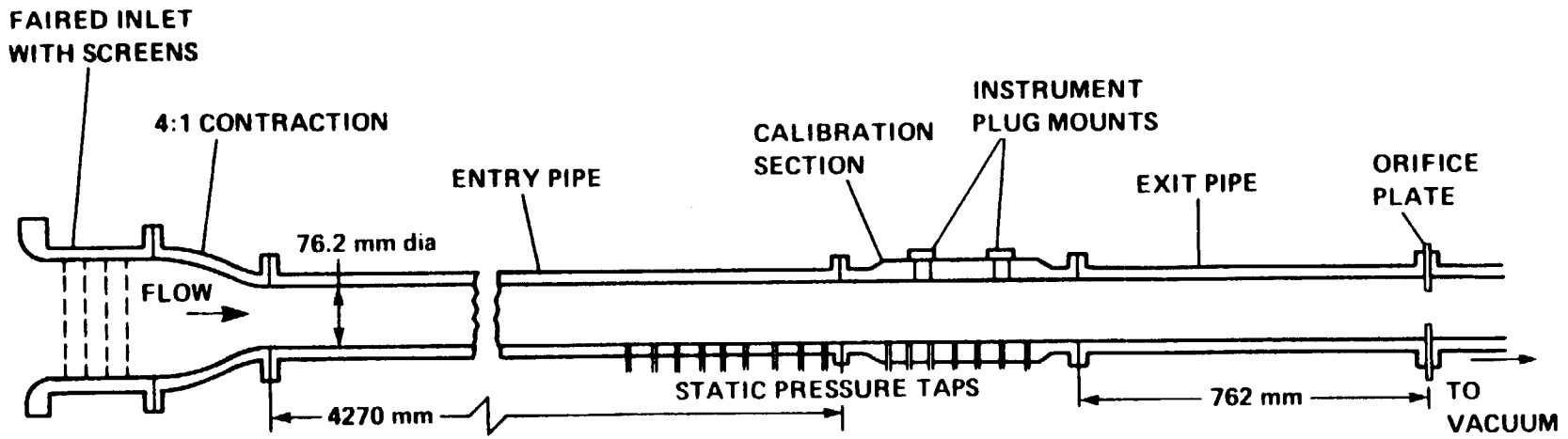

SCHEMATIC OF THE APPARATUS

Figure 19. SCHEMATIC OF PIPE FLOW AND PIPE-FLOW APPARATUS

ORIFICE = 71 mm dia; Re = 690000; CENTERLINE MACH NO. = 0.674

SYMBOL	RUN #		p_{ref}, atm	M_{ref}
○	4	SCANIVALVE, PAROS DATA	0.656	0.677
□	5	SCANIVALVE, PAROS DATA	0.654	0.678
◇	9	SCANIVALVE, PAROS DATA	0.652	0.680
△	10	SCANIVALVE, PAROS DATA	0.652	0.680
◺	11	SCANIVALVE, PAROS DATA	0.651	0.681
⬠	12	SCANIVALVE, PAROS DATA	0.651	0.681
▽	15	SCANIVALVE, PAROS DATA	0.661	0.671
———		PARABOLIC CURVE FIT, p/p_{ref}	0.654	0.675
———		M/M_{ref} (CALCULATED)	0.654	0.675
- - - - -		PARO STATIONS		

ORIFICE = 66 mm dia; Re = 620000; CENTERLINE MACH NO. = 0.568

SYMBOL	RUN #		p_{ref}, atm	M_{ref}
○	4	SCANIVALVE, PAROS DATA	0.731	0.570
□	5	SCANIVALVE, PAROS DATA	0.730	0.571
◇	9	SCANIVALVE, PAROS DATA	0.728	0.572
△	10	SCANIVALVE, PAROS DATA	0.728	0.572
◺	11	SCANIVALVE, PAROS DATA	0.728	0.571
⬠	12	SCANIVALVE, PAROS DATA	0.727	0.573
▽	15	SCANIVALVE, PAROS DATA	0.736	0.566
———		PARABOLIC CURVE FIT, p/p_{ref}	0.730	0.570
———		M/M_{ref} (CALCULATED)	0.730	0.570
- - - - -		PARO STATIONS		

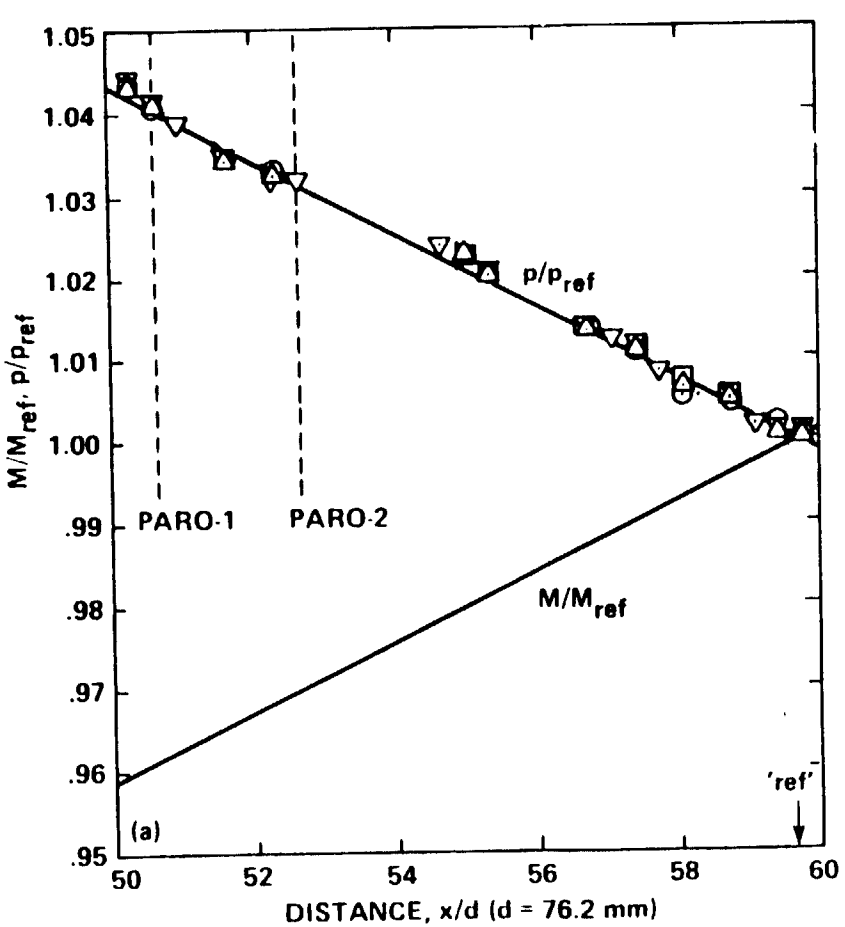

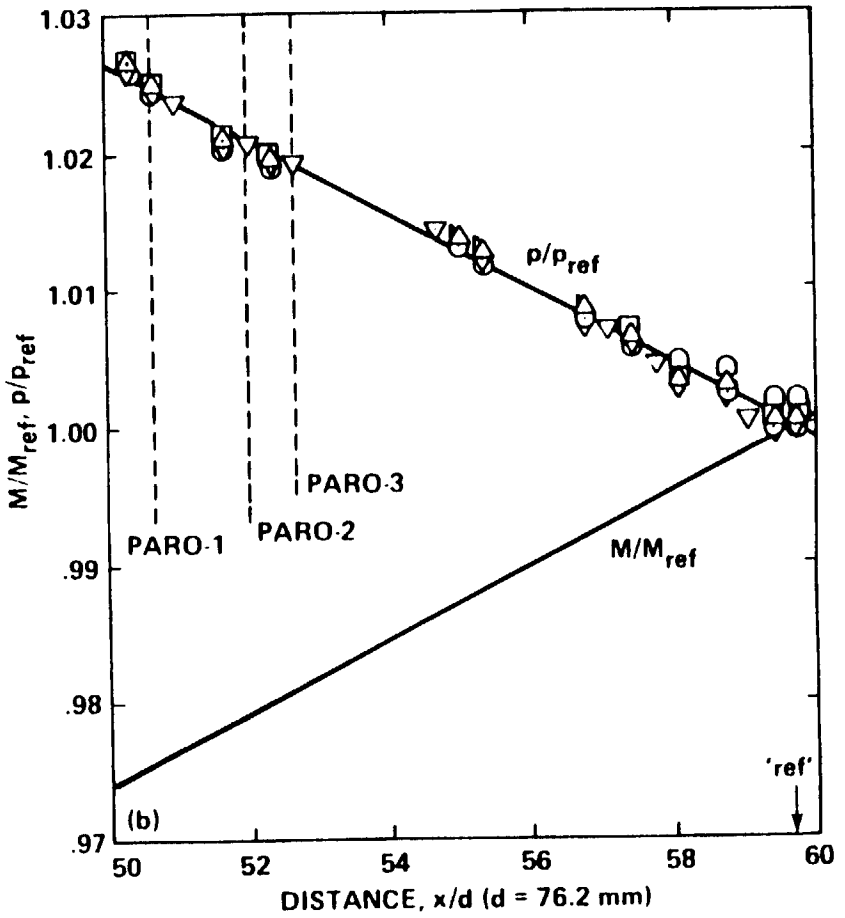

Figure 20. PRESSURE DISTRIBUTION DATA FROM PIPE-FLOW EXPERIMENTS

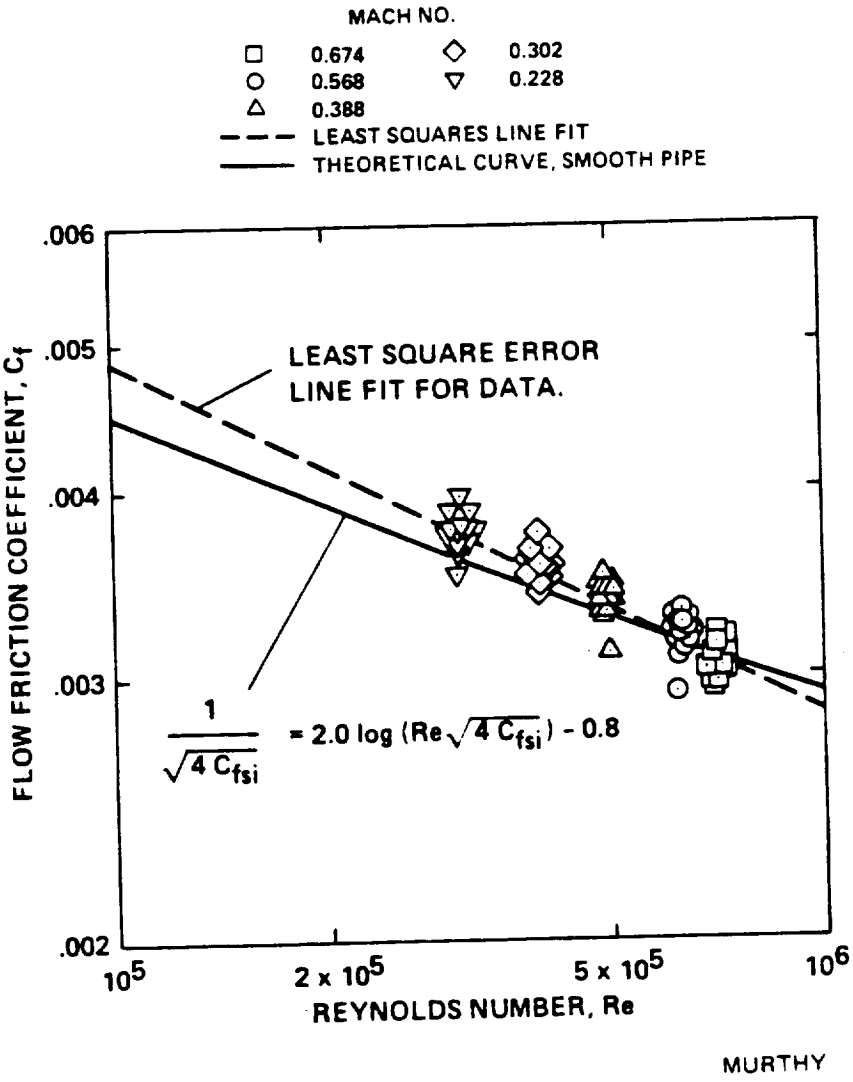

Figure 21. PIPE-FLOW FRICTION COEFFICIENT AS A FUNCTION OF REYNOLDS NUMBER

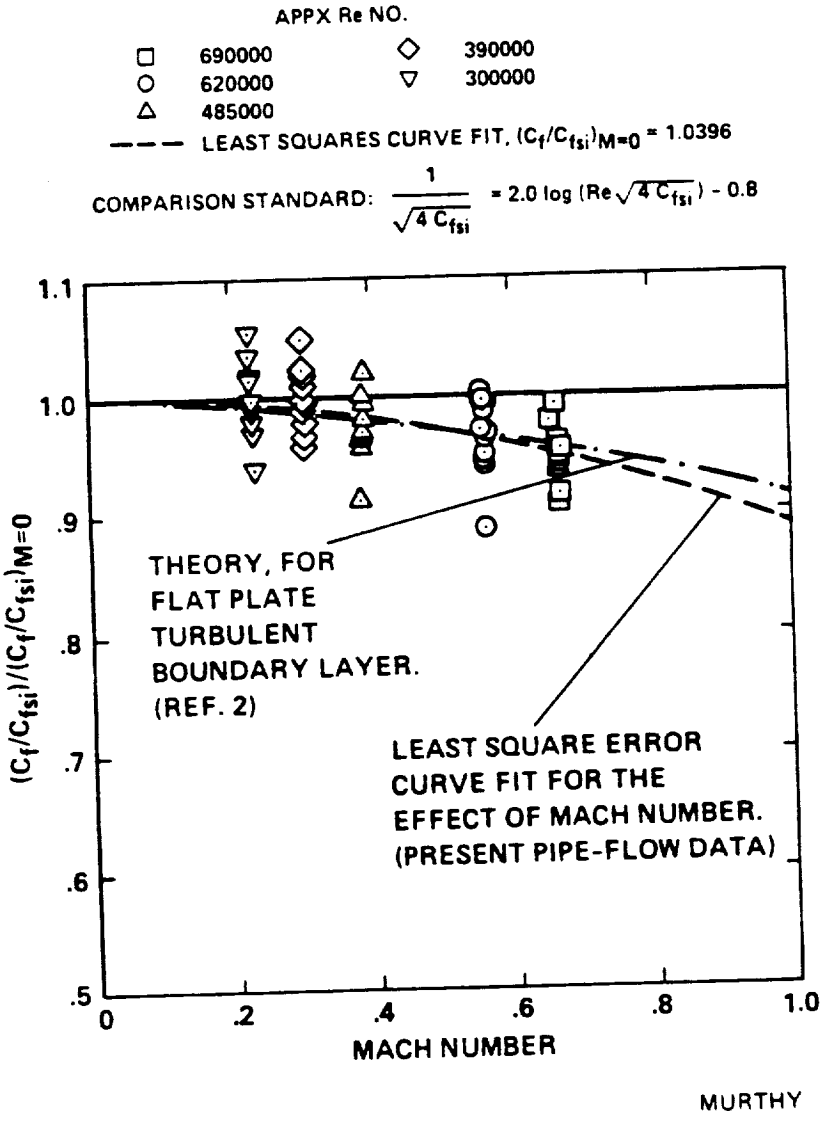

Figure 22. EFFECT OF COMPRESSIBILITY ON PIPE-FLOW FRICTION COEFFICIENT

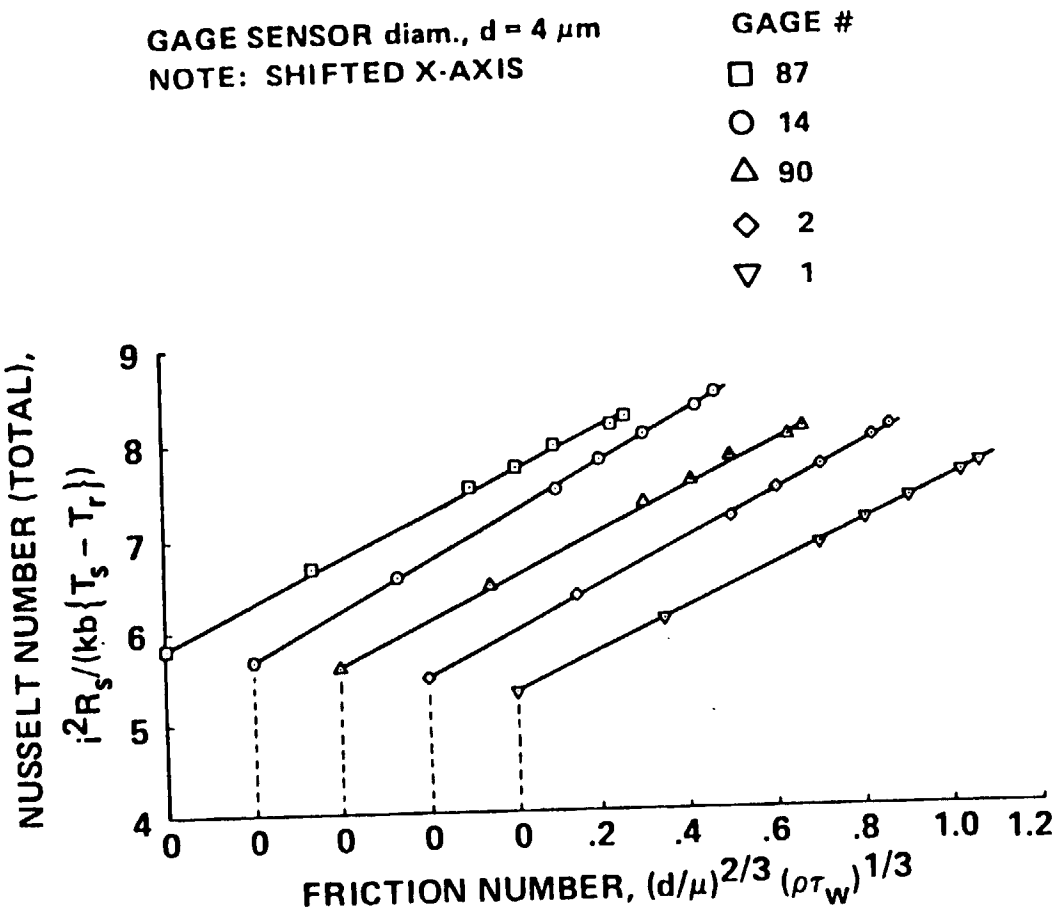

Figure 23. CALIBRATION OF BURIED WIRE GAGES - NUSSELT NUMBER vs. FRICTION NUMBER

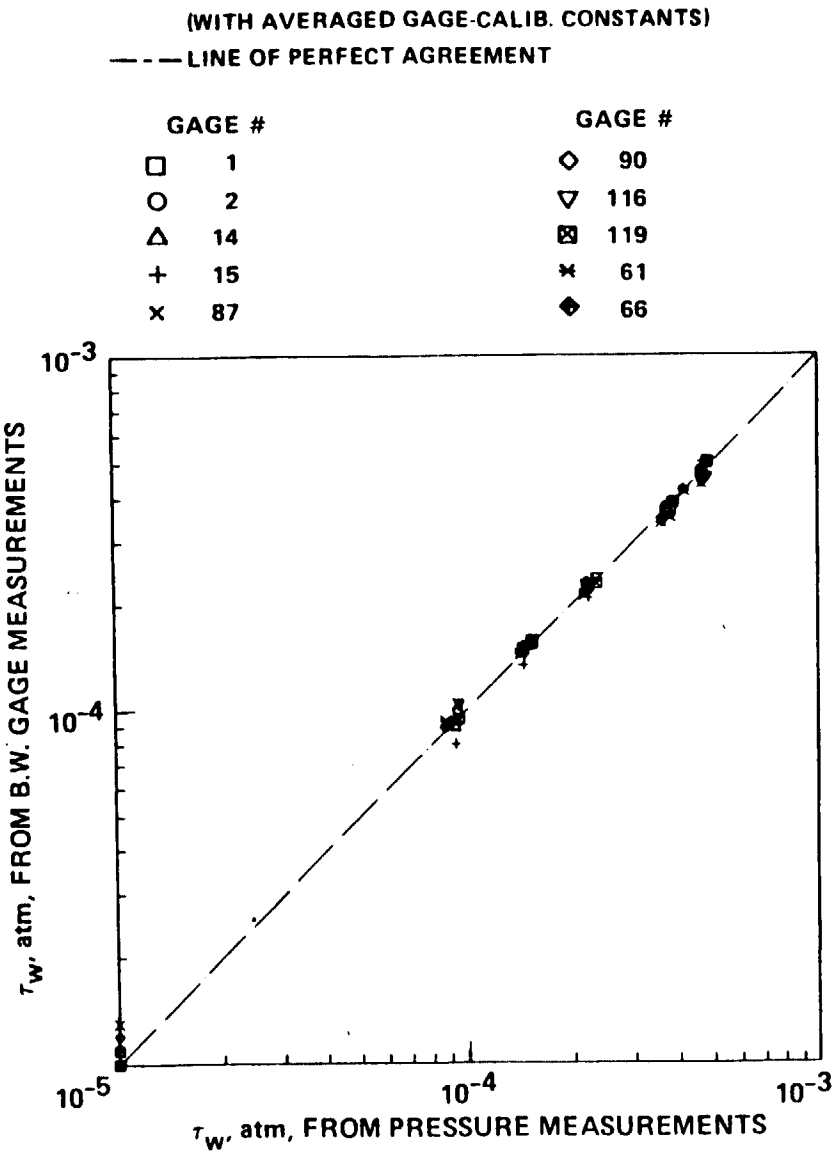

Figure 24. BURIED WIRE GAGE CALIBRATION CHECKS

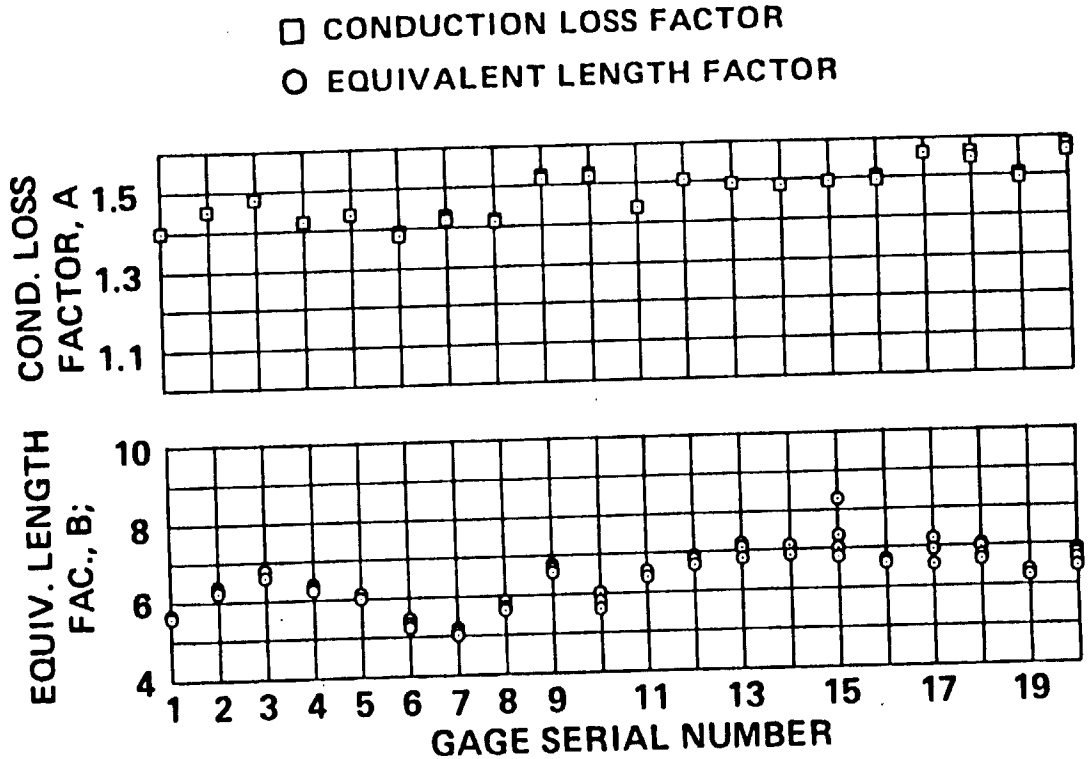

Figure 25. CALIBRATION CONSTANTS OF TYPICAL BURIED WIRE GAGES

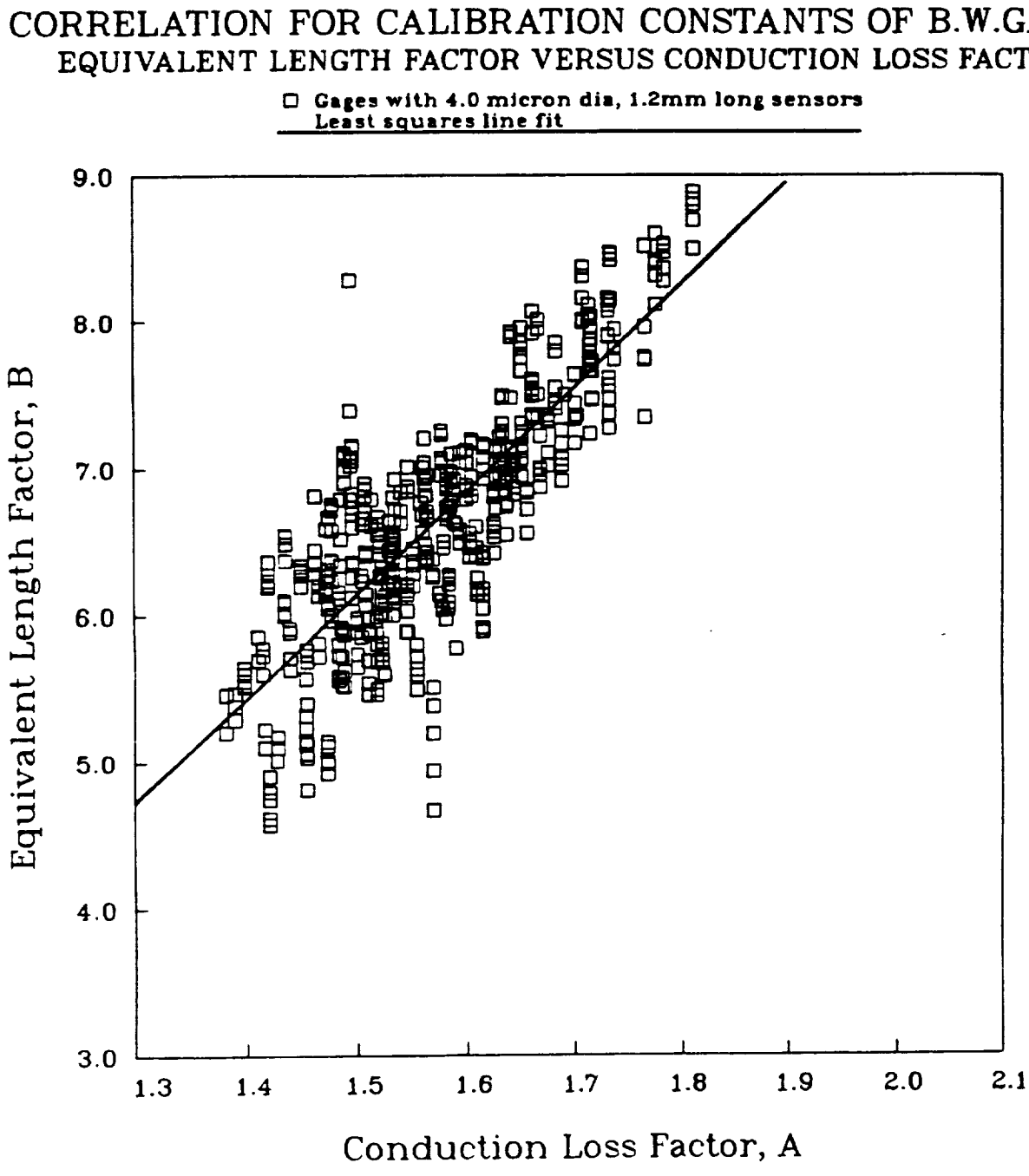

Figure 26. CORRELATION FOR CALIBRATION CONSTANTS OF BURIED WIRE GAGES

PRESSURE TRANSDUCERS IN INSTRUMENT PLUGS OF BOUNDARY LAYER APPARATUS FOR SUBSONIC AND TRANSONIC FLOWS AFFECTED BY NOISE ENVIRONMENT

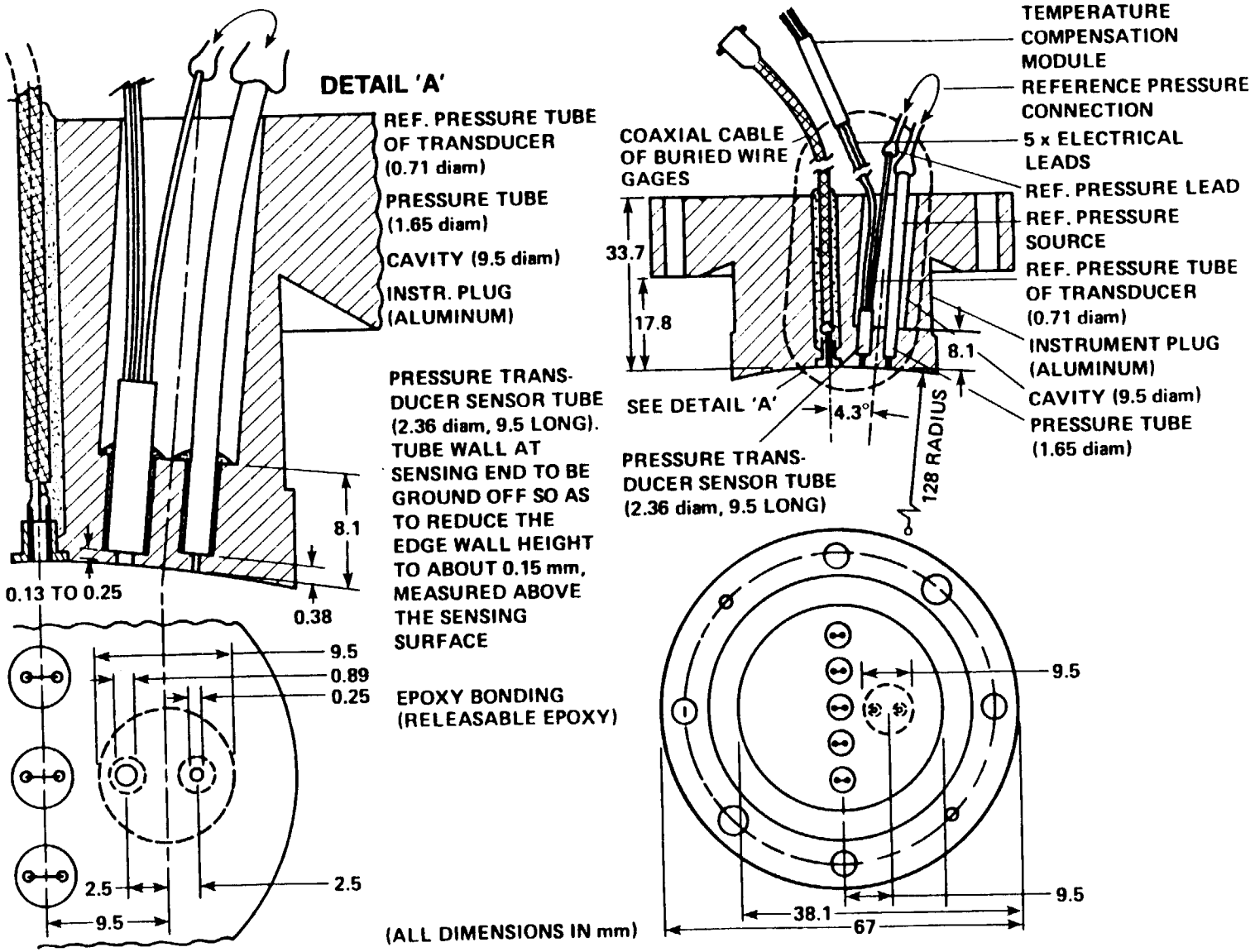

Figure 27. BURIED WIRE GAGES AND PRESSURE TRANSDUCERS IN INSTRUMENT PLUG BLANK.

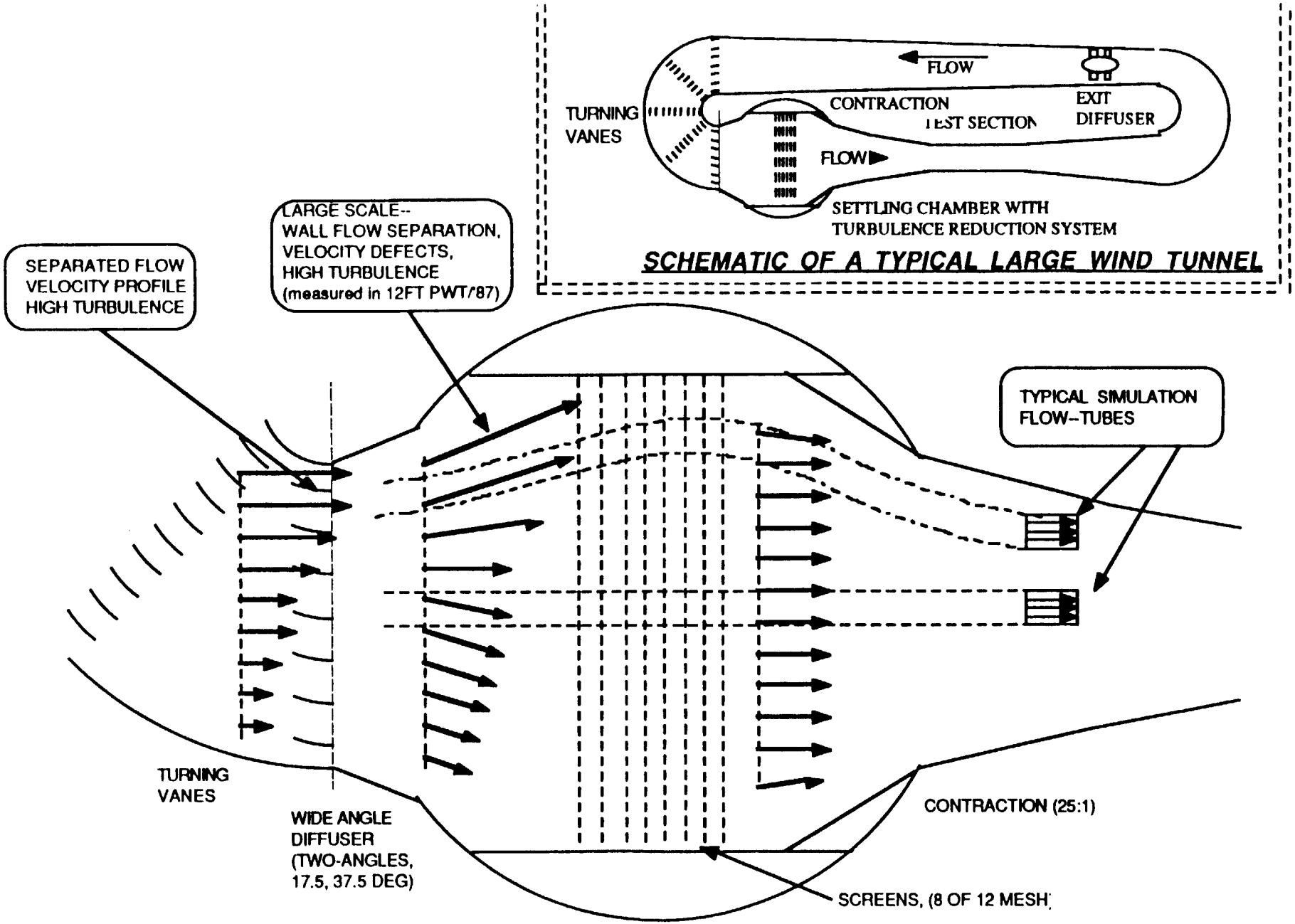

Figure 28.

SCHEMATIC OF TYPICAL FLOW PATTERN IN THE SETTLING CHAMBER OF A LARGE WIND TUNNEL

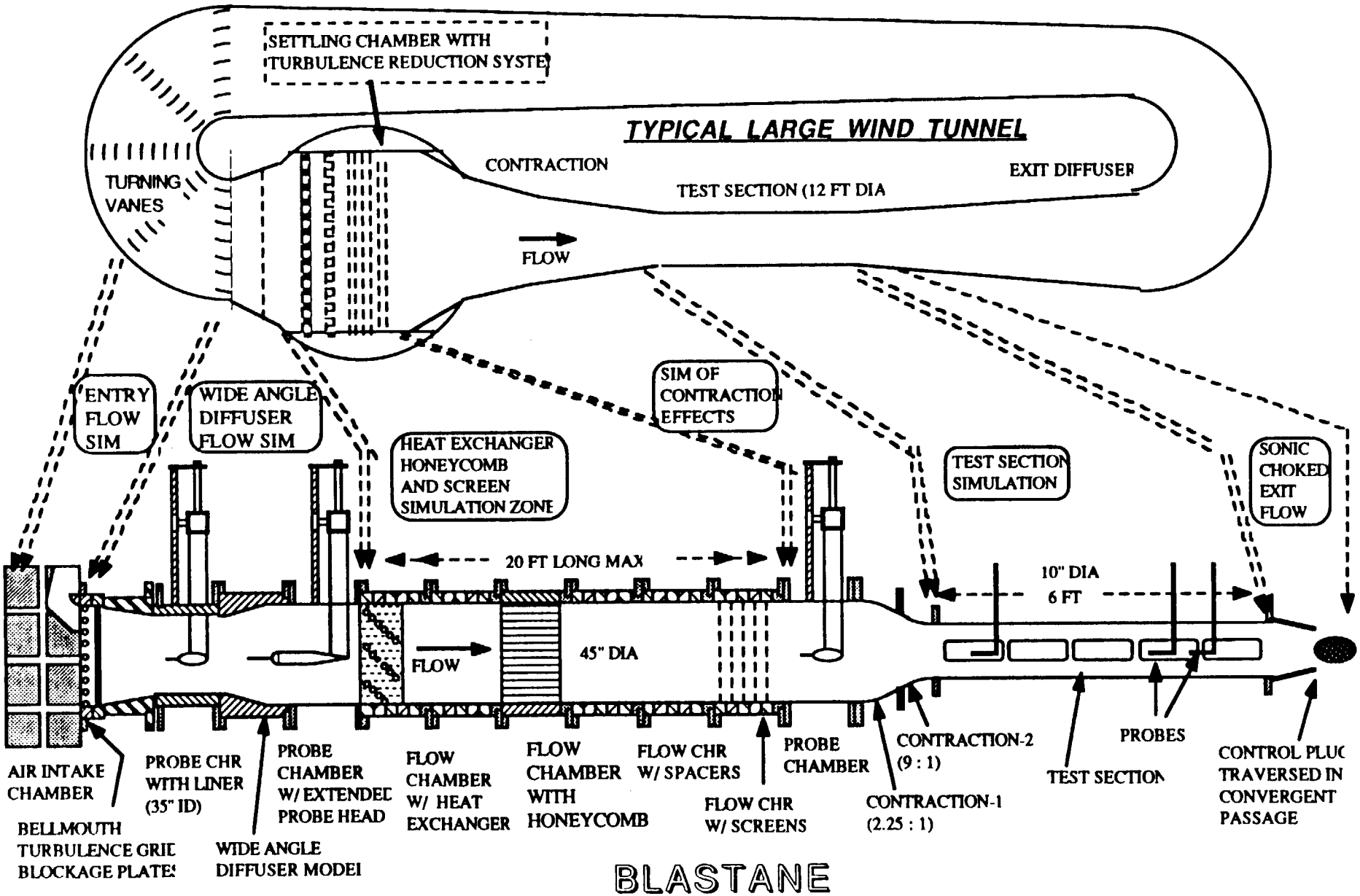

(Boundary Layer Apparatus for Subsonic and Transonic flow Affected by Noise Environment)

SCHEMATIC OF THE BLASTANE SIMULATION CONCEPT FOR STUDIES OF WIND TUNNEL FLOW QUALITY DATA BASE.

Figure 29.

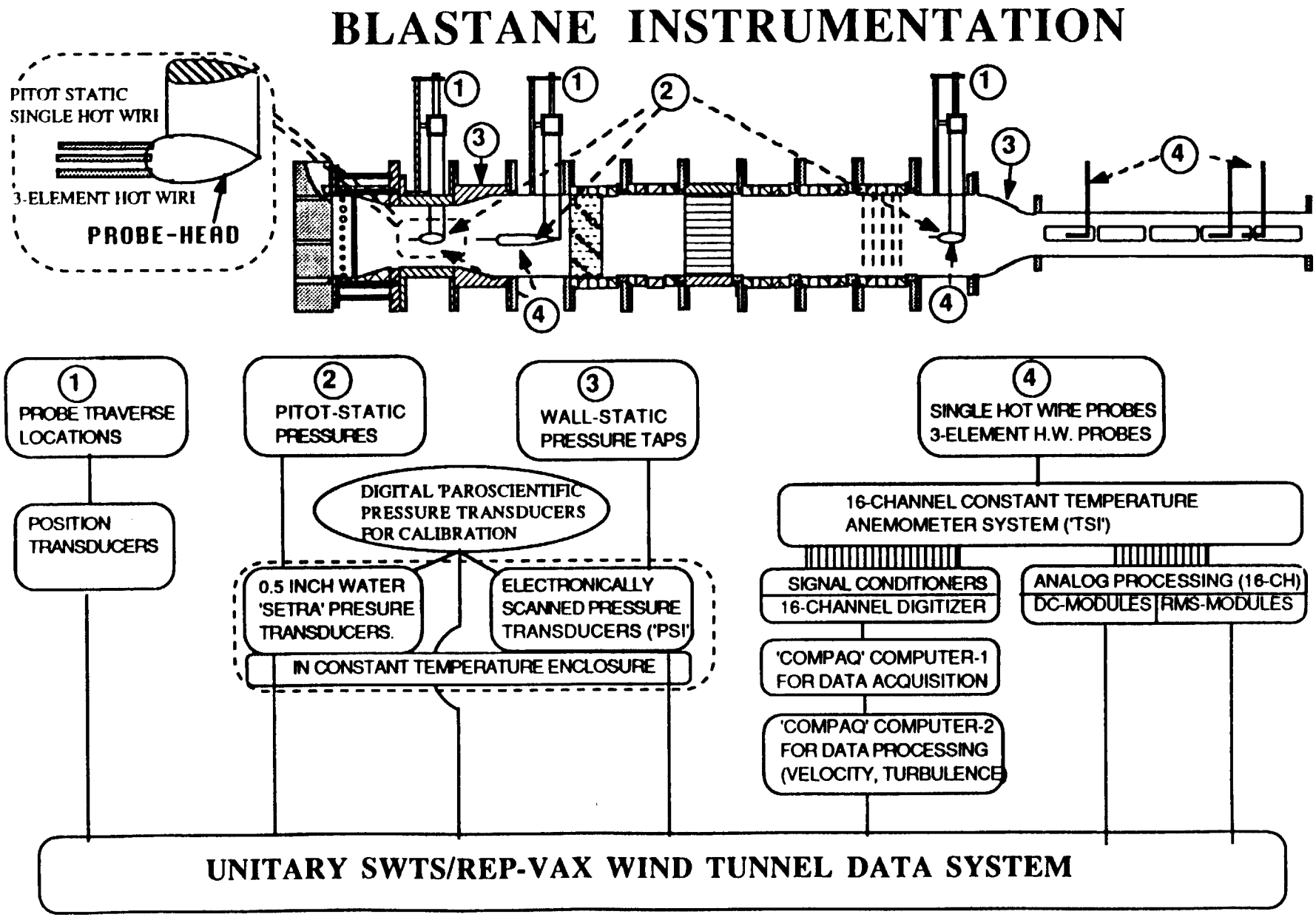

Figure 30. SCHEMATIC OF INSTRUMENTATION FOR FLOW CHRACTERIZATION TESTS

FLOW ANGLE INSTRUMENTATION

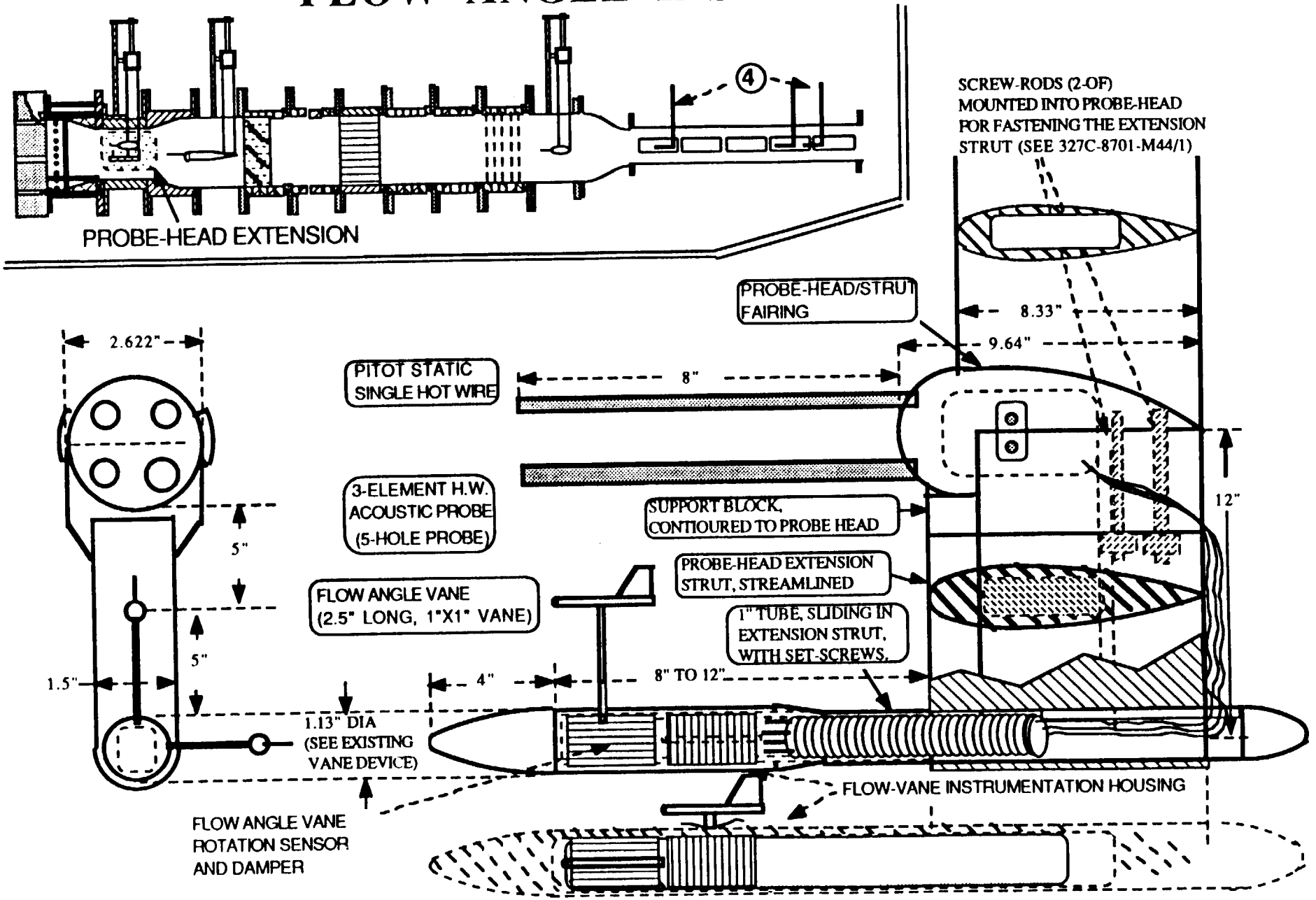

Figure 31. DETAILS OF FLOW ANGLE INSTRUMENTATION FOR FLOW CHARACTERIZATION TESTS

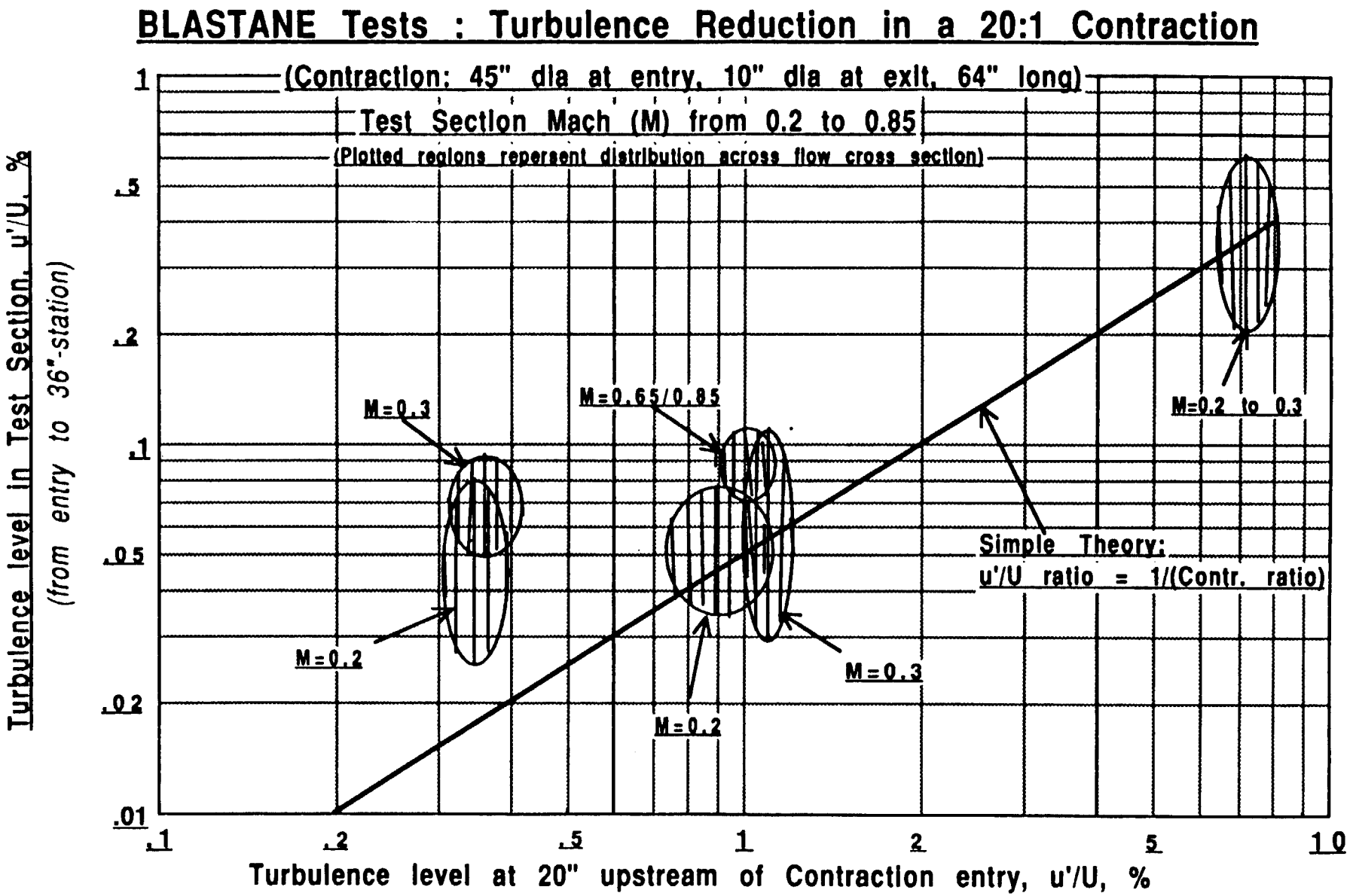

Figure 32. TURBULENCE REDUCTION THRU CONTRACTION

Data from "contr-turb/red.tbl"